Desalination and Water Treatment
www.deswater.com
doi: 10.5004/dwt.2021.27509

232 (2021) 67–90
August

Experimental and simulation investigation on the characteristics and performance of the spray separation tower for evaporation crystallization of saline wastewater

Jing Yu[a,b,*], Liang Chen[b,c], Weidong Yan[a]

[a]*School of Intelligent Engineering Technology, Jiangsu Vocational Institute of Commerce, No. 180 Longmian Avenue, Jiangning District, Nanjing 211199, China, Tel. +86 18251853848; email: 18251853848@163.com (J. Yu), Tel. +86 18963611729; email: 1153628146@qq.com (W. Yan)*
[b]*School of Energy Science and Engineering, Nanjing Tech University, No. 30 Puzhu Road(S), Nanjing 211800, China, Tel. +86 18751945135; email: chen_liang08@163.com (L. Chen)*
[c]*Yancheng Institute of Technology, No. 1 Hope Avenue Middle Road, Yancheng 224051, China*

Received 12 January 2021; Accepted 7 June 2021

ABSTRACT

Spray separation tower is the most important component in solar air circulation evaporating separation system for saline wastewater treatment. In order to explore the necessary conditions for the separation process and improve the overall system performance, the heat and mass transfer performance and evaporation crystallization characteristics of the tower are investigated through computational fluid dynamics simulation and experiment. The results reveal that the four-stage model has high accuracy in predicting the spray separation process. The air temperature has the greatest influence on the evaporation separation process of the spray separation tower. Sufficient air inlet temperature ($t_{a,\text{in}}$ > 90°C at 20% concentration) is the basic condition to ensure the curing crystallization of the wastewater droplets. However, the improvement of air temperature is not conducive to the energy utilization ratio (EUR) and η_Q of the tower. Therefore, it is necessary to maintain a certain air inlet temperature (at 20% concentration, 105°C > $t_{a,\text{in}}$ > 90°C) to ensure a high EUR (maintained above 40%, maximum of 43.78%) and η_Q (maintained above 70%, maximum of 71.97%). In addition, the increase of the mass concentration of wastewater is beneficial to the spray separation process and the solidification of particles, but it leads to the decrease of the EUR.

Keywords: Spray separation; Saline wastewater treatment; Mass transfer; Evaporation characteristics

1. Introduction

1.1. Background

With the gradual advancement of global sustainable development and ecological civilization construction, the requirements of clean and pollution-free industrialization are also gradually raised. Industrial wastewater is one of the three major sources of pollution in the process of industrial production. Its reasonable disposal can effectively reduce the diffusion and transmission of wastewater pollution and prevent its damage to the ecological environment [1]. As a typical representative of industrial wastewater, saline wastewater mainly contains various metal salt ions, such as sodium ions and calcium ions. Some saline wastewater even contains heavy metal ions, such as chromium ions and cadmium ions [2–4], which would seriously harm the ecological environment and the health of residents if improperly treated and discharged into the water source.

* Corresponding author.

Therefore, in order to reduce the possible saline wastewater leakage and improper discharge on the environmental impact, "saline wastewater "zero discharge" has gradually become the pursuit of researchers in the field of saline wastewater treatment and "zero discharge" has also become the future development trend of saline wastewater treatment.

1.2. Evaporation separation method

The evaporation separation method is an effective method to achieve "zero discharge" treatment of saline wastewater. The evaporation separation method relies on evaporation or volatilization to evaporate the water from the wastewater solution to achieve the separation effect. This physical separation method has a wide range of treatment, strong treatment capacity and low requirement for wastewater types. In addition, evaporated water and separated heavy metal salt can be recycled. The traditional evaporation separation method, namely the direct evaporation method, has some disadvantages such as high energy consumption, high-temperature requirement and low recovery efficiency of water and salt in wastewater. With the development of evaporative separation technology, the current evaporative separation methods in the industry mainly include the multi-effect distillation method [5], the mechanical vapor recompression [6] method, humidification and dehumidification (HDH) [7] and the spray evaporation separation method [8]. Among these evaporation separation methods, as an energy-saving, economical and effective method for treating saline wastewater, spray evaporation separation technology is popular because of its good dehydration effect, fast granulation speed, direct separation, and meeting the requirements of "zero discharge" for saline wastewater treatment.

1.3. Spray evaporation separation technology

Spray evaporation separation technology is widely utilized in the field of evaporation drying and solution separation, such as milk powder, fertilizer, and powder [9]. The saline solution is atomized into countless tiny droplets which leads to the great increase of the heat and mass transfer area between solution and air. Hence, the solution can be dried into solid particles in a very short time. As the spray evaporation separation technology is marked by great dehydration effect, the fast granulation speed and direct separation, the problems of evaporation equipment scaling and corrosion can be solved effectively for the application of spray evaporation separation technology in the treatment of saline wastewater.

Nowadays, spray evaporation separation technology is mainly applied to recycle the salt and curable components including various common salt impurities (such as $CaCl_2$ and Na_2SO_4) and various heavy metal salts (such as $CrCl_3$ and $Pb(NO_3)_2$) in the wastewater. Zhang et al. [10] applied the spray evaporation separation technology into the production of lignin superfine powder from the pulping waste liquor and study the performance characteristics of the system. Rouissi et al. [11] utilized the response surface methods to optimize the spray evaporation separation process and developed a formula of Radix Aucklandiae power produced from starch industrial wastewater. The results show that the cell activity of fungi did not decrease significantly. Additionally, Chasekioglou et al. [12] proved that it is an effective way to produce free-flowing powdered food from olive factory wastewater by taking the mixture of maltodextrin and air as an evaporation medium. However, the traditional spray evaporation separation technology has disadvantages such as high energy consumption and poor economic benefits. Chen [13] proposed a novel electroplating wastewater treatment system that combined spray evaporation separation technology and heat pump. The results revealed that the application of a heat pump resulted in a great decrease in the energy consumption of the system, the evaporation efficiency of this system is 32% higher than that of the direct heating system. However, the heat pump still needs to be driven by electric energy, so its primary energy utilization rate has not been significantly improved.

Compared with the combination of heat pump and spray evaporation separation technology, solar energy as a kind of clean energy, when combined with spray evaporation separation technology, can effectively reduce the dependence of the evaporation separation system on electricity, thereby reducing the consumption of primary energy. Normally, solar energy can be utilized as a heat source for spray evaporation separation technology to heat the air, which reduces the consumption of fossil energy and the operation cost of the whole evaporation separation system. Solar energy is usually combined with spray evaporation technique for seawater desalination [14], especially combined with HDH technology [15]. Since both saline wastewater and seawater are essentially brine solutions, the evaporation processes of the two are similar. Therefore, the application of spray separation technology combined with solar energy in the water-salt separation of saline wastewater also has broad prospects. Farahbod et al. [16] pointed that it is extremely important to recycle the salt and pure water for the zero-discharge treatment of saline wastewater. In recent years, some researchers have begun to devote themselves to exploring the research and application of solar-spray evaporation separation systems in the field of separation and treatment of saline wastewater [17,18]. Nevertheless, there are some unavoidable defects in these systems, such as the high inlet air temperature (above 120°C) and the requirement of vacuum degree. However, in industrial applications, the operating temperature of conventional solar collectors is often lower than 120°C, and although the vacuum conditions can lower the operating temperature, the system needs to provide additional electrical energy to maintain the vacuum. Therefore, there is still a vacancy in the investigation of the spray evaporation separation process under the operating temperature of conventional solar heat collectors (60°C~120°C).

1.4. Motivation of this work

According to the literature review in Sections 1.2 and 1.3, spray evaporation separation technology is a reliable evaporation separation method for saline wastewater, which can directly evaporate the water in the wastewater solution at one time to precipitate solid crystal salts. This technology realizes the simultaneous recovery of water

and salt in saline wastewater. Therefore, the feature of spray separation technology just meets the current urgent need for "zero discharge" of salty wastewater. However, the current spray evaporation separation system for saline wastewater has the problems of large primary energy consumption, low system efficiency and high air inlet temperature. Although the spray evaporation separation system combined with solar energy can effectively improve the system's dependence on primary energy. Researches on the spray separation process under the medium and low-temperature conditions (air inlet temperature range of 60°C~120°C) corresponding to the commonly used solar collectors are still scarce. Many researches of spray separation process focus on the system with high inlet temperature or vacuum condition, but the system performance of spray separation process with normal inlet air temperature (below 120°C) and ambient pressure has been seldom investigated. Therefore, the research on the spray evaporation separation process for the treatment of saline wastewater in the low and medium temperature range needs to be filled.

The saline wastewater spray separation tower investigated in this paper is further research of the spray separation tower in the solar air circulation evaporation separation system for the treatment of salty wastewater proposed by our research group [19] for the first time, and the system diagram is shown in Fig. 1. The system relies on solar energy as the heat source, air as the carrier, and adopts a two-stage model of low-temperature concentration and medium-temperature separation. The system can adapt well to the changes brought about by solar radiation and ensure the recovery of metal salts and water in salty wastewater. The combination of solar energy and two-stage treatment also makes the system green, clean and highly energy efficient. In our previous research literature, the heat and mass transfer performance of the spray concentration tower in the system was discussed in detail. However, the object of this article, the spray separation tower, is different from the spray concentration tower. The function of the spray separation tower in the whole system is to realize the whole process from the evaporation of wastewater to the precipitation of solutes and the formation of crystalline salt through the spray evaporation separation process of the higher concentration of saline wastewater concentrated by the spray concentration tower. Therefore, in comparison with the spray concentration process and the spray separation process in this system, the spray separation process is obviously more complicated. Except for the evaporation process caused by the convection process of wastewater droplets and air, which is the same as the spray concentration process, the wastewater droplets in the spray separation process would gradually precipitate solid crystals in the latter stage, and the crystalline product would be wrapped on the surface of the droplets which significantly changes the evaporation process of the heat and mass transfer (The droplet changes from a pure liquid state to a liquid-solid two-phase state, and the evaporation process of the droplet's mass transfer to the air will also be weakened).

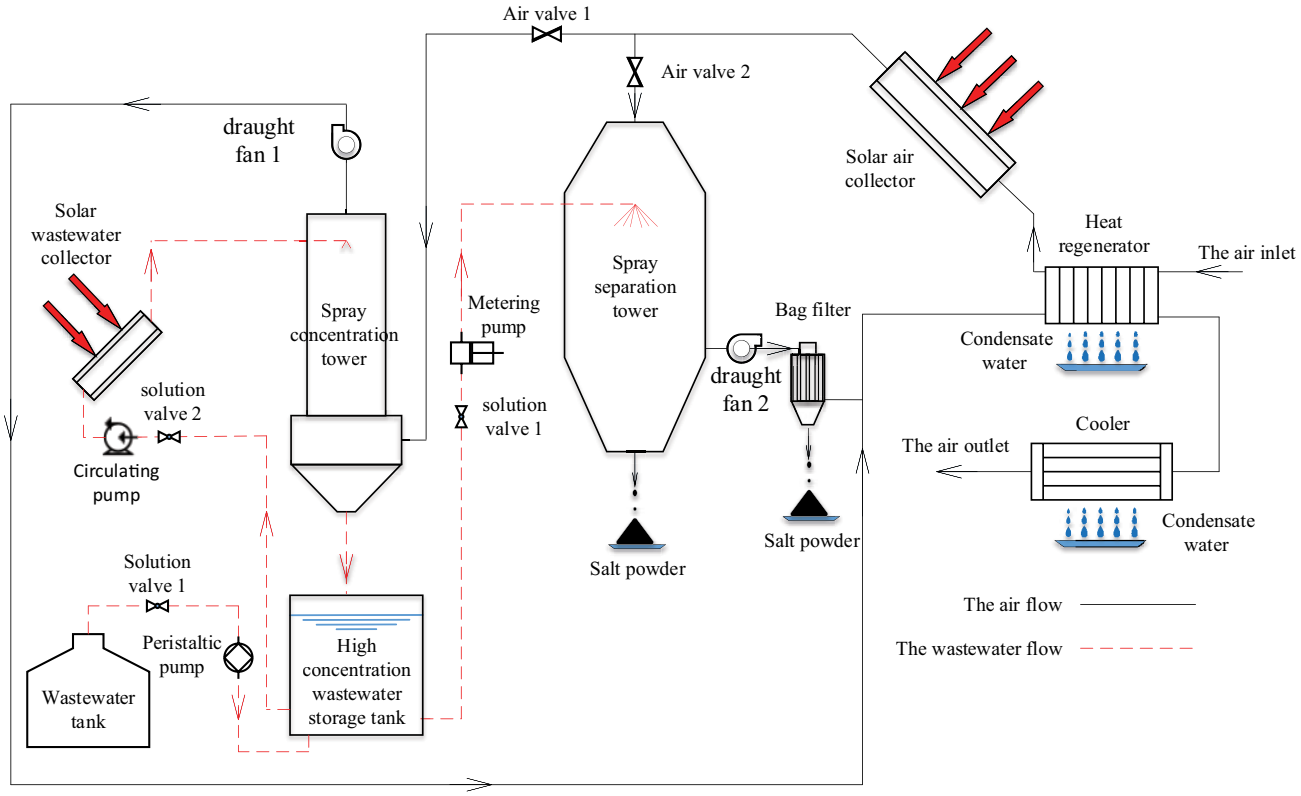

Fig. 1. The diagram of the spray separation tower in solar air circulation evaporating separation system for saline wastewater treatment.

Thus, the spray separation process model at this stage can no longer continue to use the spray concentration process model used in the previous study.

Consequently, in this paper, a four-stage model of the spray separation process combined with computational fluid dynamics (CFD) simulation is proposed, and the evaporation crystallization characteristics and performance of the spray separation tower for saline wastewater are investigated through both simulation method and experiment method. Through the investigation of the characteristics and performance of the saline wastewater spray separation tower in this work, the following two goals can be achieved:

- Reveal the evaporation and crystallization characteristics and performance change rules of saline wastewater in the spray evaporation separation process at medium and low temperatures (60°C~120°C), so as to fill the research gaps.
- Through the study of the salinity wastewater recovery part, provides a research basis for the further research of solar air circulation evaporating separation system for saline wastewater treatment.

2. Experiment

2.1. Structure of spray separation tower

Similar to the spray concentration process, the spray separation process is also the heat and mass transfer process between air and droplets. Both of them have commonness, however, there are also obvious differences. Although wastewater is atomized and the gas phase utilizes air as a carrier gas to absorb the water vapor in the droplets, unlike the spray concentration process, the spray separation process requires the droplets to be vaporized and dried to a solid-state (in the form of salt hydrates). Hence, in order to ensure the effective progress of the spray separation process, the design of the spray separation tower has special requirements for the provided air temperature, the atomization effect of the droplets, and the gas–liquid flow ratio.

Therefore, relevant adjustments need to be made in the design of the spray separation tower structure. In order to ensure that the process can complete the separation of water and salt, a smaller droplet diameter and higher air inlet temperature are required. The smaller droplet diameter means that the drag force of the discrete droplet in the gas phase is relatively stronger. Therefore, in order to effectively recover heavy metal salt powder in wastewater, the flow pattern must be changed from counter-current to downstream. In addition, in order to increase the residence time of the discrete phase in the tower and ensure that the height of the tower does not exceed the scope of industrial implementation, the diameter of the main body of the tower was appropriately increased. The specific structure diagram of the spray separation tower is shown in Fig. 2.

The spray separation tower is divided into two layers, the upper structure is made of stainless steel, the lower layer is made of polyacrylate material consistent with the spray separation tower, and the two layers are connected by a flange. Due to the high air inlet temperature at the top of the tower, this two-layer result form is

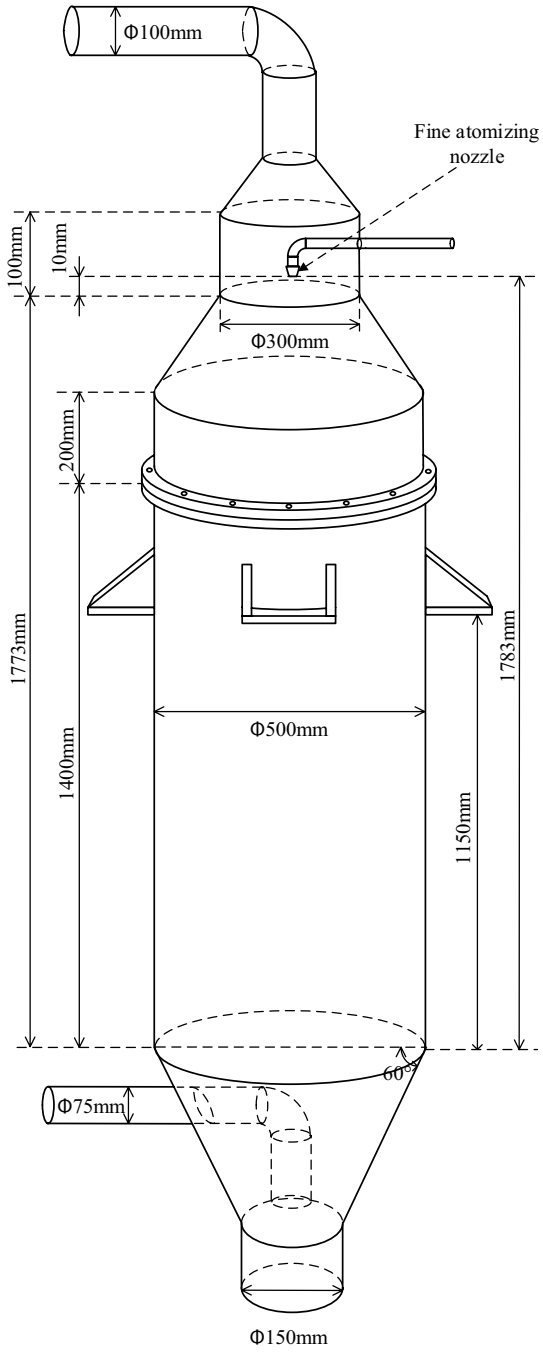

Fig. 2. Structure diagram of the spray separation tower.

chosen to balance visualization and temperature resistance. According to the recommended aspect ratio of the spray separation tower (greater than 1.5:1) in the literature [24], the size of the spray separation tower in this study is designed as shown in Fig. 2, the effective evaporation height of the spray separation tower is 1,783 mm (as shown in Fig. 2, this size is made up of the sum of the lengths of four parts, which are the vertical cylinder height of the lower part of the spray separation tower 1,400 mm, the height of the upper part of the tower 200 mm, the height of the slope of the upper part of the tower 173 mm and the

distance from the nozzle mouth to the plane of the cylinder 10 mm), while the diameter of the main evaporation separation area is 500 mm. In addition, like the spray concentration tower, the spray separation tower is coated with 20 mm thickness of thermal insulation cotton for integral thermal insulation treatment. At the top of the tower, a fine atomizing pressure swirl nozzle with a plastic inset ceramic inner core is adopted. The nozzle chooses a fine atomizing nozzle model KBN80063 produced by Shanghai Dianrui Machinery Technology Co., Ltd. (Shanghai, China), with an orifice diameter of 0.2 mm. The specific performance parameters of this type of nozzles are shown in Table 1.

Rated pressure and rated flow rate are 0.5 MPa and 1.07 L h^{-1} respectively, and spray tension angle is 50°. The bottom of the tower body is provided with a downward bending air outlet pipe, which can increase the output of dry crystal salt directly recovered from the bottom of the tower and facilitate the collection of the test process.

2.2. Experimental system of the spray separation tower

According to the spray separation tower designed in Section 2.1, the corresponding spray separation tower performance experiment platform was built, and the heat and mass transfer and evaporation separation performance of the separation tower are tested and studied. The experiment system is shown in Fig. 3.

The spray flow direction of the spray separation tower is the same as that of airflow. Since the spray evaporation separation technology used in this paper is one of

Table 1
Specific performance parameters of KBN nozzles

Type	Orifice diameter (mm)	Flow rate (L h^{-1}) at pressure (MPa)				Spray angle (°) at pressure (MPa)			
		0.5 MPa	1 MPa	1.5 MPa	2 MPa	0.5 MPa	1 MPa	1.5 MPa	2 MPa
KBN80063	0.2	1.07	2	2.62	3.12	50	80	80	80
KBN80125	0.3	2.19	4.1	5.37	6.39	60	80	80	80
KBN80022	0.4	3.88	7.25	9.49	11.3	65	80	80	80

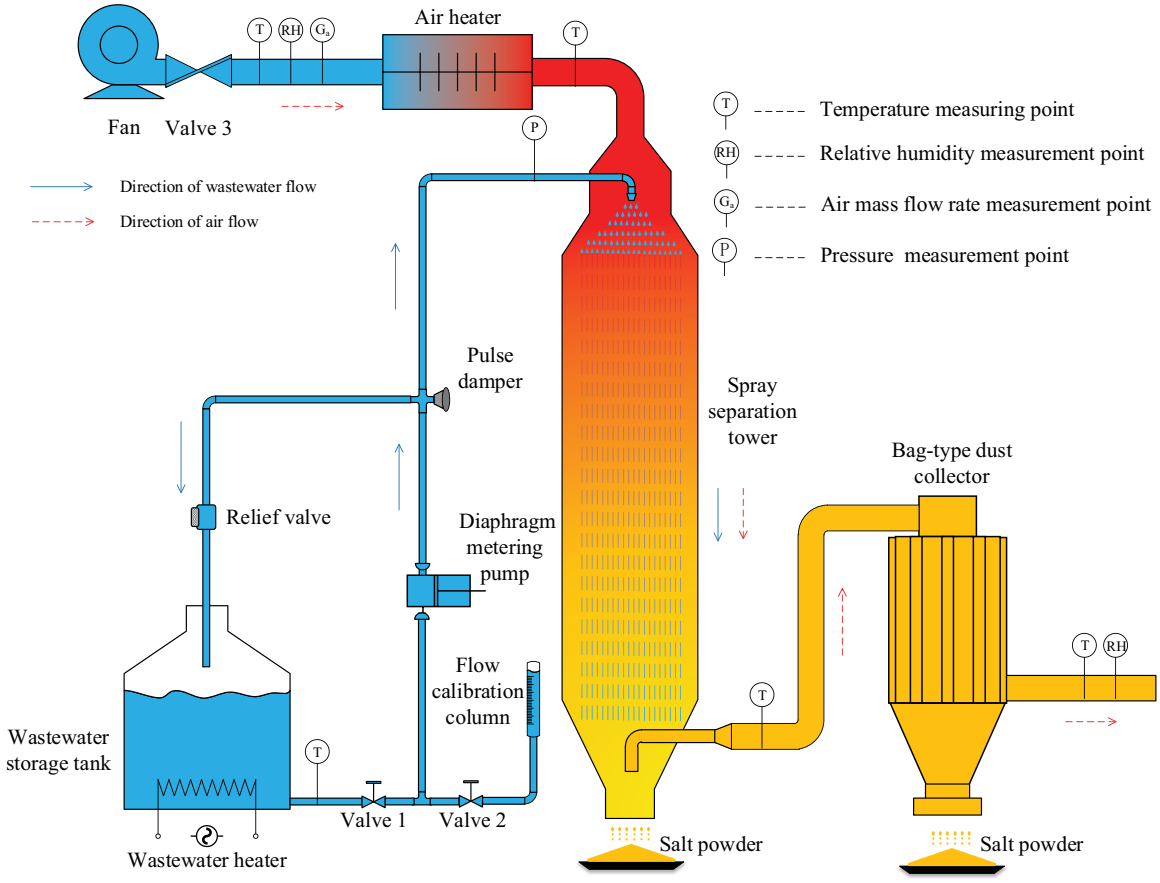

Fig. 3. Experimental system diagram of spray separation tower.

the evaporation separation methods, the difference in the composition and type of wastewater itself has a relatively small impact, but the mass concentration of wastewater has a relatively large impact on the evaporation separation process. Therefore, the selection of calcium chloride solution as the research object in this experiment has certain representativeness. Calcium chloride is a common component of industrial salt-containing wastewater. For example, in the chemical process of preparing phosphoric acid, calcium chloride is the most common component of process wastewater products. Its thermodynamic parameters can be obtained by the study of Moffat [20]. In addition, this experiment tests a variety of working conditions, and the mass concentration of wastewater is taken as an important measurement index. In the control experiment of wastewater mass concentration, the performance of the spray separation tower was studied under the change of wastewater mass concentration from 0 to 40% (detail in Section 2.3).

The main components of the test system include a spray separation tower, air heater, bag filter, wastewater heater, liquid storage tank, fan, diaphragm metering pump and its accessories. The diaphragm metering pump with a lower flow rate and higher pressure is selected to spray the waste liquid, and the pulse damper and relief valve can ensure the continuous and stable liquid supply of the wastewater in the spray flow path. The function of the bag filter is to filter out the crystal salt particles carried in the airflow at the outlet of the tower. Considering the corrosion problem and the pressure resistance problem, the spray flow path is made of polyethylene material with a reinforcing rib. The airflow path is consistent with the spray concentration tower test platform, and the air duct with aluminum foil inside is used to connect each component, and 30 mm insulation cotton material is wrapped outside the air duct. The actual experimental system and data observation in the experimental process are shown in Fig. 4. The yellow arrows in Fig. 4 correspond to several important components in the experimental system of Fig. 3, and the red dotted arrows indicate the direction of airflow during the operation of the experimental system. In addition, the data

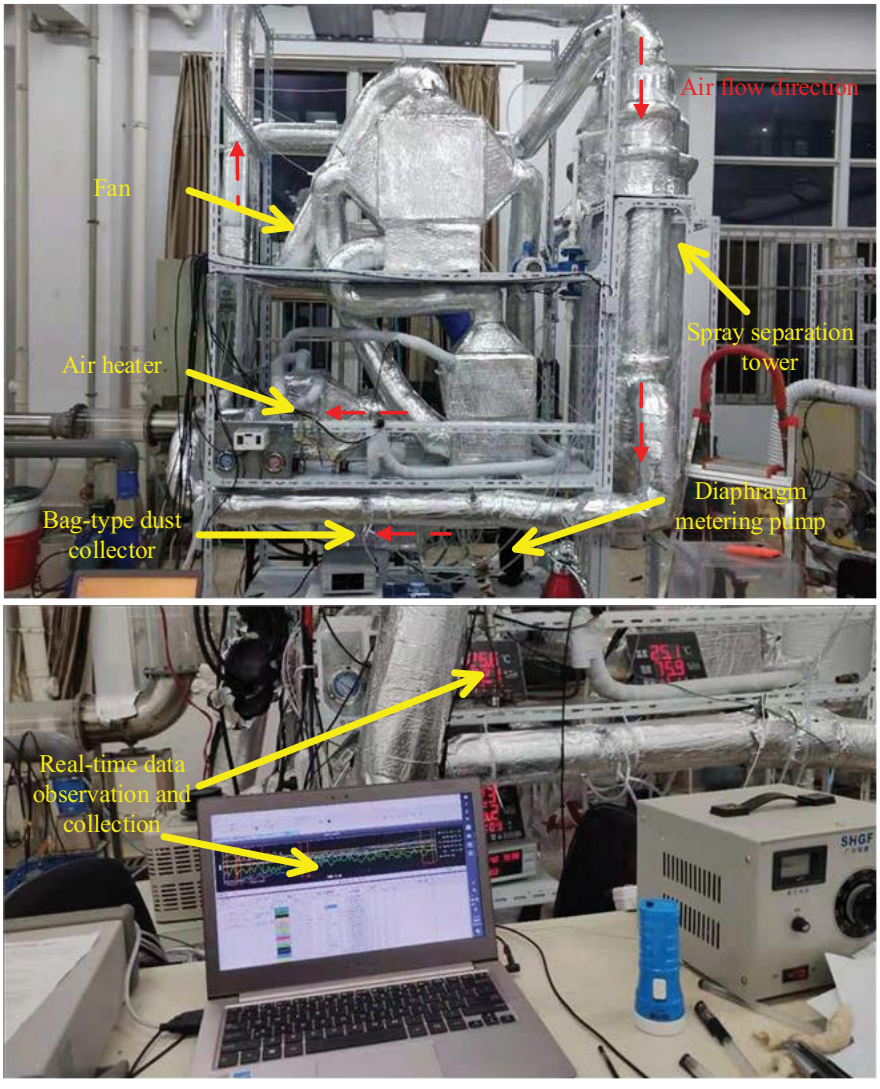

Fig. 4. Physical photo of spray separation tower experimental system.

acquisition instrument is connected with the computer to display the changes of the parameters of each state point, so as to monitor the experiment process in real-time.

The specific measuring instruments and measurement accuracy are listed in Table 2. Although the diaphragm metering pump can be roughly read out its spray flow, the accuracy deviation is large. Therefore, a flow calibration column was arranged in the spray flow path, and the spray flow was indirectly measured by measuring the time of the wastewater solution being sucked away by the diaphragm pump. Since the spray separation tower uses a fine atomizing nozzle with a single spray hole with a smaller aperture, its spray pressure is higher, so a pressure sensor with a higher range is needed for pressure measurement.

During measurement, each group of experimental conditions begins to measure readings after the state parameters are basically stable. Each data is read once every 2 min for a total of 3 times, and the average value is calculated as the experimental measurement results under this working condition.

Meanwhile, according to the method suggested by Moffat [20], uncertainty in measurement is defined as the root sum square of the instrumental fixed errors and the random errors observed in different measurements. In addition, since the uncertainty of the directly measured quantity in this experiment can be regarded as mutually independent, the uncertainty of indirect parameters is calculated as follows:

$$u_c=\sqrt{\sum_{i=1}^{N}\left(\frac{\partial f}{\partial x_i}\right)^2\left(u_{xi}\right)^2} \tag{1}$$

where x represents direct measurement parameters, f is the relationship between indirect parameters and direct parameters, and u_x stands for the error of direct measurement values. According to the above method, the uncertainty of each calculated parameter is calculated using the uncertainty propagation function in Engineering Equation Solver (EES).

2.3. Experimental conditions

The main influencing factors of evaporation and crystallization characteristics of spray separation tower are inlet air temperature, air mass flow rate, inlet wastewater temperature, wastewater mass flow rate and wastewater mass concentration. Therefore, this experiment is carried out to force on these five factors. The experimental method of spray separation tower is a controlled variable method and the experimental conditions are shown in Table 3. The experimental groups 1 to 5 in the table respectively represent the control variable experiments of the above five influencing factors. For example, experimental group 1 represents the effect of inlet air temperature on the performance of the spray separation tower (by keeping other influencing factors unchanged, changing the inlet air temperature, and measuring the changes in the spray separation tower outlet parameters under different inlet air temperatures, so as to get the change of the performance of the spray separation tower with the inlet air temperature).

2.4. Experimental steps

The experimental research can be carried out according to the above experimental conditions. In order to ensure the reliability of the measured data, the following experimental operation steps are mainly followed:

2.4.1. Preparation stage:

(1) According to the requirements of the different operating conditions, prepare the corresponding concentration of calcium chloride solution and keep stirring to fully

Table 2
Measuring instrument and precision of spray separation tower experimental system

Parameters	Measuring device	Instrument type	Precision	Measuring range
Temperature	Pt100 Platinum Resistance Thermometer	WZP-270	–	–200°C–420°C
Relative humidity	Electronic humidity sensor	LX-868	±3% RH	0%–100%
Air mass flow rate	Pressure differential meter	HSTL-FY01	±0.25% FS	0~50 Pa
Wastewater mass flow rate	Flow calibration column	SS304-100	±1 mL	0~100 mL
Spray pressure	Pressure transducer	MIK-P300	±0.3% FS	0~1 MPa

Table 3
Experimental conditions

Parameters	1	2	3	4	5
t_0, °C	22.7 ± 0.1	22.7 ± 0.1	23.1 ± 0.1	23.1 ± 0.1	23.1 ± 0.1
$w_{a,in}$, g kg^{-1}	8.714 ± 0.1	8.714 ± 0.1	8.8578 ± 0.1	0.8578 ± 0.1	0.8578 ± 0.1
$t_{a,in}$, °C	60~120	105 ± 0.1	105 ± 0.1	105 ± 0.1	105 ± 0.1
$t_{w,in}$, °C	22.7 ± 0.1	22.7 ± 0.1	25~65	23.1 ± 0.1	23.1 ± 0.1
m_d, kg h^{-1}	95.1 ± 1	55~115	95.1 ± 1	95.1 ± 1	95.1 ± 1
m_w, kg h^{-1}	1.93 ± 0.02	1.93 ± 0.02	1.93 ± 0.02	1.72~3.53	1.93 ± 0.02
x_{in}, %	20	20	20	20	0~40

dissolve the solid calcium chloride. After standing for a whole, filter insoluble impurities from the solution for reserve use;
(2) Power on all measuring instruments, turn on the computer, turn on the data acquisition instrument, record the zero point of the pressure differential meter, the ambient temperature and the ambient relative humidity;
(3) Inject the prepared calcium chloride solution into the wastewater storage tank. Open valve 1, close valve 2 and open diaphragm pump in turn. Observe whether there are fog drops in the tower after a period of time (if there are no fog drops, close the diaphragm pump and release pressure in time, and check whether the spray pipeline is blocked);

2.4.2. Experiment stage:

(1) After the pressure of the spray pipeline stabilizes, open valve 2 and close valve 1 to fill the solution into the flow calibration column, then record the time required to pump out all the solutions in the flow calibration column. After testing the wastewater flow rate, open valve 1 and close valve 2;
(2) Open valve 3, fan and electric heater in turn. Then adjust rheostat and valve 3 to the specified air temperature and the airflow rate;
(3) When the outlet air temperature and relative humidity of the spray separation tower no longer change, observe whether there is solid precipitation in the outlet of the tower, record one set of the inlet and outlet state parameters under this condition every 2 min for total 3 times.
(4) Adjust the parameters that need to be changed under this working condition group, and repeat the experiment stage step (3) until the end of the experimental test under this working condition group;

2.4.3. Closing stage:

(1) Turn off the electric heater until the inlet air temperature drops below 40°C and turn off the fan;
(2) Replace the calcium chloride solution in the wastewater storage tank with clear water, clean the solution pipe and the spray separation tower for more than 10 min. Then close the diaphragm pump and open the pressure relief valve to relieve pressure;
(3) Save the data recorded by the data acquisition instrument;
(4) Turn off the power supply of the experimental system.

2.5. Experimental data processing

After collecting the test data, the test data of each group were sorted out and the performance parameters were calculated. The performance tests of the spray separation tower include:

Evaporation rate of spray separation tower wastewater m_e:

$$m_e = m_d\left(w_{a,\text{out}} - w_{a,\text{in}}\right) \tag{2}$$

Water content x_d of crystalline salt particles at the outlet of spray separation tower (fog drops if crystallization is not possible):

$$x_d = \frac{m_w(1-c) - m_e}{m_w - m_e} \tag{3}$$

Evaporation efficiency of spray separation tower EE:

$$\text{EE} = \frac{1{,}000m_e}{C_{p,w}\left(m_{w,\text{in}}T_{w,\text{in}} - m_{w,\text{out}}T_{a0}\right) + m_d\left(h_{a,\text{in}} - h_{a0}\right)} \tag{4}$$

Energy utilization of spray separation tower EUR_{ss}:

$$\text{EUR} = \frac{m_e L_{\text{av}}}{C_{p,w}\left(m_{w,\text{in}}T_{w,\text{in}} - m_{w,\text{out}}T_{a0}\right) + m_d\left(h_{a,\text{in}} - h_{a0}\right)} \tag{5}$$

Specific air consumption (SAC):

$$\text{SAC} = \frac{m_d}{m_d\left(w_{a,\text{out}} - w_{a,\text{in}}\right)} \tag{6}$$

Thermal efficiency η_Q:

$$\eta_Q = \frac{m_e L_{\text{av}}}{C_{p,w}\left(m_{w,\text{in}}T_{w,\text{in}} - m_{w,\text{out}}T_{w,\text{out}}\right) + m_d\left(h_{a,\text{in}} - h_{a,\text{out}}\right)} \tag{7}$$

3. Dynamic model of the spray separation tower

In order to study the heat and mass transfer and the dry separation characteristics of the spray separation process inside the tower, a dynamic model is established for the main flow of the spray separation tower using ANSYS Fluent 15.0.

3.1. Physical model

Firstly, the mesh model of the spray separation process as shown in Fig. 5 is established according to the structure size of Fig. 2. The grid model of the spray separation tower also adopts the modeling form of the axisymmetric model under cylindrical coordinates. However, the nozzle of the spray separation tower adopts a single nozzle instead of a form of porous parallel jet flow. Therefore, the wastewater needs to be in the form of a point trigger into the spray separation tower. Fig. 4 shows the nozzle position of the pressure cyclone used in the spray separation tower. In addition, the quadrilateral grid is adapted to encrypt the part near the wall, and ICEM software is used to draw the grid model. The total mesh number of the spray separation tower mesh model is 391425.

3.2. Continuous phase (air) model

The airflow in the spray separation tower is a continuous turbulent flow. Therefore, based on the Navier–Stokes equation, the continuity equation and momentum equation in the case of cylindrical coordinates are expressed in the following form.

Continuity equation:

$$\frac{\partial \rho_a}{\partial \tau} + \frac{\partial}{\partial x}\left(\rho_a v_x\right) + \frac{\partial}{\partial r}\left(\rho_a v_r\right) + \frac{\rho_a v_r}{r} = S_m \tag{8}$$

where ρ_a is the air density while v_x and v_r represent axial and radial gas phase velocities respectively. S_m is a user-defined

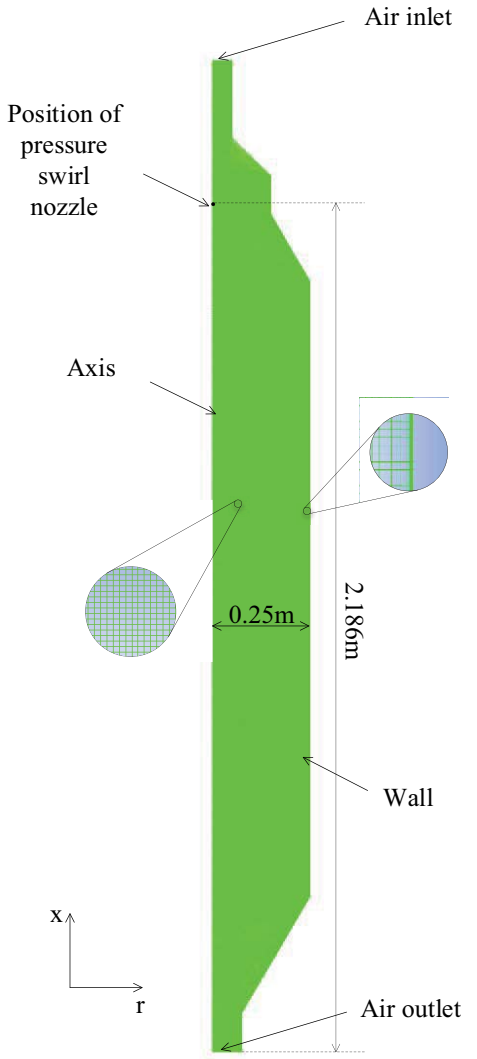

Fig. 5. Mesh diagram of the spray separation tower.

source term and it typifies the source term of discrete phase droplets.

Axial momentum equation:

$$\frac{\partial}{\partial\tau}\left(\rho_a v_x\right)+\frac{1}{r}\frac{\partial}{\partial x}\left(r\rho_a v_x v_x\right)+\frac{1}{r}\frac{\partial}{\partial r}\left(r\rho_a v_r v_x\right)=-\frac{\partial P}{\partial x}+\frac{1}{r}\frac{\partial}{\partial x}\left[r\mu_a\left(\frac{2\partial v_x}{\partial x}-\frac{2}{3}\left(\nabla\cdot v_a\right)\right)\right]+\frac{1}{r}\frac{\partial}{\partial r}\left[r\mu_a\left(\frac{\partial v_x}{\partial r}+\frac{\partial v_r}{\partial x}\right)\right]+F_x \tag{9}$$

Radial momentum equation:

$$\frac{\partial}{\partial\tau}\left(\rho_a v_r\right)+\frac{1}{r}\frac{\partial}{\partial x}\left(r\rho_a v_x v_r\right)+\frac{1}{r}\frac{\partial}{\partial r}\left(r\rho_a v_r v_r\right)=-\frac{\partial P}{\partial x}+\frac{1}{r}\frac{\partial}{\partial x}\left[r\mu_a\left(\frac{\partial v_r}{\partial x}+\frac{\partial v_x}{\partial r}\right)\right]+\frac{1}{r}\frac{\partial}{\partial r}\left[r\mu_a\left(\frac{2\partial v_r}{\partial r}-\frac{2}{3}\left(\nabla\cdot v_a\right)\right)\right]-2\mu_a\frac{v_r}{r^2}+\frac{2}{3}\frac{\mu_a}{r}\left(\nabla\cdot v_a\right)+F_r \tag{10}$$

In this two-momentum equation, $\nabla\cdot v_a$ represents the velocity gradient, and its expression is:

$$\nabla\cdot v_a=\frac{\partial v_x}{\partial x}+\frac{\partial v_r}{\partial r}+\frac{v_r}{r} \tag{11}$$

In the above equation, P stands for pressure and μ_a represents the air viscosity. F_x and F_r represent additional forces acting in the axial and radial directions.

Turbulent viscosity can be calculated by:

$$\mu_t=C_\mu\rho_a\frac{k^2}{\varepsilon} \tag{12}$$

Above, μ_t represents turbulent viscosity, C_μ is the constant of the equation, k stands for turbulent kinetic energy and ε typifies energy dissipation.

3.3. Discrete phase (wastewater droplets) model

Similar to the spray concentration process [19], the spray separation process can also be regarded as the heat and mass transfer process between the continuous phase air and the discrete phase wastewater droplets. However, since the spray separation process would generate dry crystalline salt products, and the heat and mass transfer process will significantly change when the droplet gradually changes from the liquid phase to the solid phase, it is necessary to distinguish the drying process of the droplet.

According to the literature [21], the evaporation and drying process of the droplet can be divided into four stages as shown in Fig. 6. The temperature adjustment stage and the constant temperature evaporation stage are the same as the heat and mass transfer process in the concentration process. The mathematical model of the two cases is the same, but the shell-forming stage and the drying stage are quite different. Due to the gradual formation of the solid shell, vaporization of fog drops needs to break through the outer shell, and the resistance of the mass transfer process will increase. Therefore, the evaporative drying model of fog drops in this two-stage condition needs to be given separately.

In addition, the following hypothesizes are given for liquid-phase droplets.

(1) The spray droplets are Rosin–Rammler distribution, the droplets are symmetrical spherical (each single droplet is a sphere) and the interactions between the droplets, such as collision and agglomeration, are negligible.
(2) Since the droplets are larger than 10 μm in diameter, they are not mesoscopic. Therefore, the effects of Brownian force, basset force and Saffman buoyancy are ignored.
(3) The mass, momentum and energy transmission between gas and liquid is carried out through a relative motion of the two-phase flow and heat and mass transfer.

Therefore, discrete phase droplets are affected by its own inertia, gas-phase aerodynamic drag force and gravity.

Based on the above analysis of the droplet drying stage, it is clear that the continuous (gas) phase model can follow the mathematical model of the spray concentration process, while the discrete (droplet) phase model needs to be

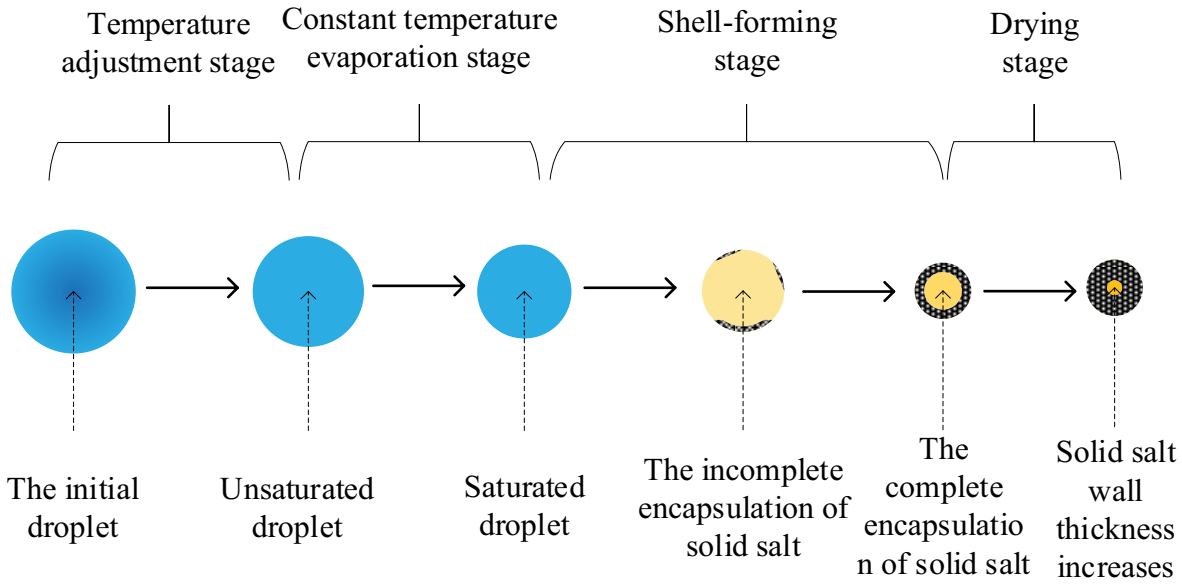

Fig. 6. Schematic diagram of the drying process of saline droplets.

supplemented. The specific model of evaporation separation of the discrete phase of a droplet is as follows:

3.3.1. Temperature adjustment stage and constant temperature evaporation stage

According to the combined Euler–Lagrangian approach, the trajectory of droplets can be obtained by the following force balance equation:

$$\frac{dv_d}{d\tau} = F_D\left(v_a - v_{\mathrm{dp}}\right) + \frac{g\left(\rho_{\mathrm{dp}} - \rho_a\right)}{\rho_{\mathrm{dp}}} \tag{13}$$

In the formula, v_d and ρ_d represent the velocity and density of droplets respectively, while g represents the acceleration of gravity. $F_D(v_a - v_d)$ is the unit mass drag force of droplets. Here F_D can be calculated by:

$$F_D = C_D \frac{18\mu_a}{\rho_{\mathrm{dp}} d_d^2} \frac{\mathrm{Re}_{\mathrm{dp}}}{24} \tag{14}$$

Thereinto, d_d is the droplet diameter. C_D and Re_d respectively represent the drag coefficient and the liquid drop relative Reynolds number, and their expressions are as follows:

$$C_D = a_1 + \frac{a_2}{\mathrm{Re}_{\mathrm{dp}}} + \frac{a_3}{\mathrm{Re}_{\mathrm{dp}}^2} \tag{15}$$

$$\mathrm{Re}_{\mathrm{dp}} = \frac{\rho_a d_d \left| v_a - v_{\mathrm{dp}} \right|}{\mu_a} \tag{16}$$

In the above formula, a_1, a_2 and a_3 are the constant and can be obtained from the literature [22]. It is assumed that the droplet is spherical with symmetry, the internal temperature distribution of a single droplet is uniform, and the effect of thermal radiation can be ignored. The heat balance equation of gas–liquid two-phase flow can be expressed as:

$$m_{\mathrm{dp}} c_p \frac{dT_{\mathrm{dp}}}{dt} = \alpha A_d \left(T_\infty - T_{\mathrm{dp}}\right) + \frac{dm_{\mathrm{dp}}}{d\tau} h_{\mathrm{fg}} \tag{17}$$

where m_{dp} is the mass of the droplet. T_d and T_∞ represent the droplet temperature and air temperature severally. C_p is the specific heat capacity of droplets and A_d is the droplet surface area. Furthermore, h represents convective heat transfer coefficient and h_{fg} is the latent heat of vaporization.

The equation of the mass transfer process is as follows:

$$\frac{dm_{\mathrm{dp}}}{dt} = -k_c A_d \left(C_{\mathrm{dp}} - C_\infty\right) \tag{18}$$

where k_c is the mass transfer coefficient. C_s and C_∞ are the moisture concentration on the surface of the droplet and in the volume of the gas respectively.

The convection heat transfer coefficient and mass transfer coefficient can be obtained by the correlation formula [23] between Nusselt number (Nu) and Sherwood number (Sh). The correlation formula is as follows:

$$\mathrm{Nu} = \frac{\alpha d_d}{\lambda_\infty} = \left(1 + B_T\right)^{-\frac{2}{3}} \left(2 + 0.552 \mathrm{Re}_{\mathrm{dp}}^{\frac{1}{2}} \mathrm{Pr}^{\frac{1}{3}}\right) \tag{19}$$

$$\mathrm{Sh} = \frac{k_c d_d}{D_m} = 2 + 0.552 \mathrm{Re}_{\mathrm{dp}}^{\frac{1}{2}} \mathrm{Sc}^{\frac{1}{3}} \tag{20}$$

Above, λ_∞ is thermal conductivity of the gas phase and D_m is steam diffusion coefficient. Pr and Sc represents Prandtl number and Schmidt number respectively, and the expressions are as follows:

$$\mathrm{Pr} = \frac{c_{p\infty}\mu_\infty}{\lambda_\infty} \tag{21}$$

$$\mathrm{Sc} = \frac{\mu_\infty}{\rho_\infty D_m} \tag{22}$$

where μ_∞, $c_{p\infty}$, ρ_∞ are gas-phase viscosity, specific heat capacity and density at constant pressure, respectively.

In addition, the vapor diffusion coefficient is the correlation equation given by the study of Mujumdar [24]:

$$D_m = 3.564\times10^{-10}\left(T_{\mathrm{dp}} + T_\infty\right)^{1.75} \tag{23}$$

where T_{dp} and T_∞ are respectively the absolute temperatures of the droplet and the absolute temperature of the gas phase.

3.3.2. Drying stage

In the drying stage, the evaporation of the wet core inside the fog drop is hindered by the outer shell because the solid crystalline salt has completely covered the surface of the fog drop. According to the literature [25], it can be assumed that the internal liquid phase wet core is in a saturated solution state, and the mass transfer coefficient k_c of fog drops at this stage is no longer only related to Sherwood number, which can be expressed as:

$$k_c = \frac{1}{\frac{d_d}{\mathrm{Sh}D_m} + \frac{d_d^2}{2D'_m}\left(\frac{1}{d'_d} - \frac{1}{d_d}\right)} \tag{24}$$

where Sh and D_m can be obtained through Eqs. (19) and (22) respectively, while the vapor diffusion coefficient D'_m and the diameter d_d of wet nucleus inside the fog drop to the solid shell can be obtained through Eqs. (24) and (25) respectively:

$$D'_m = \varepsilon_{\mathrm{cr}}^2 D_m \tag{25}$$

$$dd'_d = \frac{2W_{\mathrm{cr}}}{\pi\rho_{d\,\mathrm{sat}}d'^2_d\left(W_{\mathrm{cr}} - c_{\mathrm{sat}}\right)}dm_{\mathrm{dp}} \tag{26}$$

where $\varepsilon_{\mathrm{cr}}$ represented the porosity of the shell, $\rho_{d\,\mathrm{sat}}$ and c_{sat} represented the density and concentration of saturated wet nucleus in the droplet. The W_{cr} represented the mass fraction of crystalline salt hydrate in the solid shell. In this study, $CaCl_2$ solution as a wastewater substitute was used to produce crystals of calcium chloride dihydrate under the spray drying condition.

In addition to the change of mass transfer coefficient, as the contact surface between fog drops and air changes from the liquid phase to a solid phase, the calculation method of Nu affecting convective heat transfer also needs to be adjusted, which can be expressed as:

$$\mathrm{Nu} = \left(1 + B'_T\right)^{0.7}\left(2 + 0.6\mathrm{Re}_d^{\frac{1}{2}}\mathrm{Pr}^{\frac{1}{3}}\right) \tag{27}$$

3.3.3. Shell-forming stage

Solid and liquid substances exist on the surface of the droplets in the shell-forming stage, and the heat and mass transfer in this stage is complex. According to the literature [25], it can be known that the formation time of solid thin shell on the surface of fog drops to completely cover the surface is very short, so the heat and mass transfer process of fog drops at this stage can be regarded as the heat and mass exchange between solid crystals on the surface of z % and liquid saturated solution on the surface of 1–z % and the air.

Therefore, the mass transfer equation can be expressed as:

$$\frac{dm_{\mathrm{dp}}}{d\tau} = -A_d\left(C_d - C_\infty\right)\left[z\%\cdot k_{c,\mathrm{LQ}} + \left(1 - z\%\right)k_{c,\mathrm{SD}}\right] \tag{28}$$

$$m_{\mathrm{dp}}c_p\frac{dT_d}{d\tau} = A_d\left(T_\infty - T_d\right)\left[z\%\cdot h_{\mathrm{LQ}} + \left(1 - z\%\right)h_{\mathrm{SD}}\right] + \frac{dm_{\mathrm{dp}}}{d\tau}h_{\mathrm{fg}} \tag{29}$$

where $k_{c,\mathrm{LQ}}$ and $k_{c,\mathrm{SD}}$ represent the mass transfer coefficients of liquid and solid phases on the surface of the droplet respectively, which can be obtained from Eqs. (19) and (23), and α_{LQ} and α_{SD} represent the heat transfer coefficients of liquid and solid phases respectively, which can be obtained from Eqs. (18) and (26), respectively.

In addition, z % can be expressed as [26]:

$$dz\% = -\frac{6c_{\mathrm{sat}}dm_{\mathrm{dp}}}{\pi\rho_d\left(1 - \varepsilon_{\mathrm{cr}}\right)\left(d_d^3 - d'^3_d\right)\left(W_{\mathrm{cr}} - x_{\mathrm{sat}}\right)} \tag{30}$$

The UDF code of the four-stage drying model was written according to the above model, and the custom extension terminal in the DPM model option in fluent was used to import the code for subsequent simulation.

According to sections 3.2 and 3.3, the continuous phase model and the discrete phase model can be combined to simulate the evaporation process in the spray separation tower. What needs to be explained here is that in order to ensure the comparability of the simulation research results and the experimental research results, this simulation research adopts steady-state conditions to carry out the simulation. Therefore, in the steady-state process simulation in this study, the influence of the time term is involved in the above models [e.g., Eqs. (8)–(10), (13), (17), etc.] on the process only reflects the relative positions of air and droplets under different boundary conditions. However, this influence can be macroscopically expressed by the flow rate of air and wastewater (for example, the residence time of wastewater droplets in the tower can be obtained by the flow rate of wastewater and the geometric size of the tower).

3.4. Boundary conditions

The boundary types and boundary conditions of each boundary face of the spray separation tower are shown in Table 4. The direction of the gravitational acceleration extends along the opposite direction of the x-axis, and the value is 9.81 m s^{-2}.

The ANSYS FLUENT 15.0 software was used for simulation research. The convergence criterion adopts the most

Table 4
Boundary types and boundary conditions of spray separation tower

Boundary surface	Boundary types	DPM boundary types	Inlet temperature (K)	Inlet mass flow rate (kg h^{-1})	Inlet air humidity ratio (kg/kg dry air)	Mass concentration of wastewater (%)
Air inlet	Mass flow inlet	Escape	333.15~393.15	55~125	0.007854~0.01185	
Spray separation tower wall	Adiabatic wall	Wall film	–	–	–	–
Axis	Axisymmetric axis	–	–	–	–	–
Air outlet	Outflow	Escape	–	–	–	–
Spray point	–	Pressure swirl injection inlet	295.85~338.15	1.72~3.53	–	0~40

common residual judgment method. The convergence of simulation calculation is judged by the curve in the residual monitoring window of FLUENT. All observed absolute residual terms are set at 10^{-5}, including continuity, x-velocity, y-velocity, energy, k, ε, H_2O and O_2.

3.5. Grid independence analysis

For the simulation study of the spray separation process, the mesh independence analysis is carried out by the same method. The boundary conditions are $m_{d\ \mathrm{in}}$ = 95.1 kg h^{-1}, $m_{w\ \mathrm{in}}$ = 1.93 kg h^{-1}, $T_{a\ \mathrm{in}}$ = 378.15 K, $T_{w\ \mathrm{in}}$ = 298.15 K, w_{in} = 0.008636 kg/kg dry air, x = 20%. As shown in Table 5, the situation of different grid densities under the same boundary condition is simulated and calculated. The comparison results show that when the grid number reaches 391425, the air outlet parameters and the particle parameters of the wastewater after the spray evaporation separation process basically remain unchanged. Therefore, the physical grid model with a grid number of 391425 is adopted for subsequent simulation calculation.

In addition, Y+ value is also used for the verification of locally encrypted boundary layer grids. The RNG k–ε turbulence model and the enhanced wall function were used in the CFD simulation of the spray separation tower. So, the criteria are the same. As shown in Fig. 7, in the mainstream area (the tower height is within the range of 0.5~2.2 m), the wall Y+ value is maintained at about 1, while the inlet and outlet as well as the position where the tower diameter changes slightly fluctuate, but the overall Y+ value is also within 5. Therefore, the encryption of the wall boundary layer is also reliable.

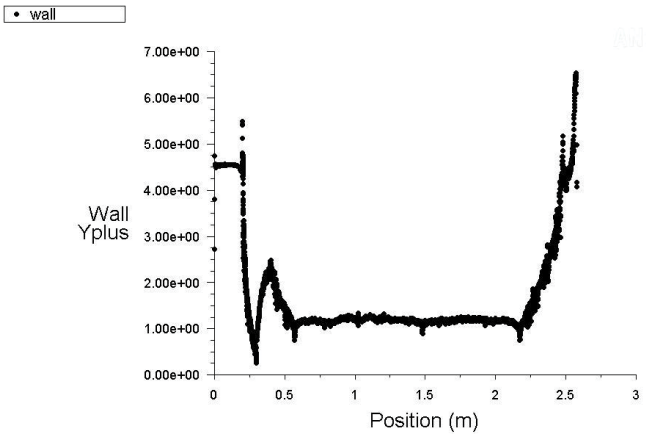

Fig. 7. Y plus on the wall.

4. Results and discussion

4.1. Model verification

The CFD simulation model of the spray separation tower is validated by comparing the simulation results with the experimental results in this section. The same boundary conditions of CFD simulation were set according to the test inlet conditions, and the direct measurement parameters of the outlet were compared. Different from spray concentration tower, because the effluent of spray separation tower is in the form of particles (or droplets), it is impossible to directly measure its temperature and moisture content. Therefore, only the air outlet parameters are compared here. The parameters such as the temperature and water content of wastewater particles were obtained indirectly by the equilibrium equation. Under different conditions, the results of wastewater parameters are given in section 4.2 analysis.

Fig. 8 shows the comparison of air outlet temperature and relative humidity of spray separation tower under all test conditions. For the air outlet temperature of the tower, the error between the predicted results of the model calculation and the test results under all working conditions is less than ±5% (the maximum error is 4.83%), while the maximum deviation of the relative humidity of the two air outlets is –5.19%, and most of them are also within ±5%. Therefore, the CFD model of the spray separation tower established in this paper is reliable and can be used to calculate and analyze the heat and mass transfer of two-phase flow in the tower which cannot be measured in the experiment.

4.2. Analysis of influencing factors

There are many factors influencing the heat and mass transfer in the spray separation column. Based on the experimental conditions, the effects of air inlet temperature,

Table 5
Comparison of simulation results under different grid densities

Number of grid	Outlet air temperature (K)	Outlet air humidity ratio (kg/kg dry air)	Outlet particle temperature (K)	Outlet particle moisture content (%)
48928	325.06	0.02351	320.05	0.2443
97857	326.59	0.02316	321.66	0.2444
195713	326.81	0.02305	321.48	0.2444
293569	326.77	0.02309	321.56	0.2444
391425	326.78	0.02310	321.54	0.2444

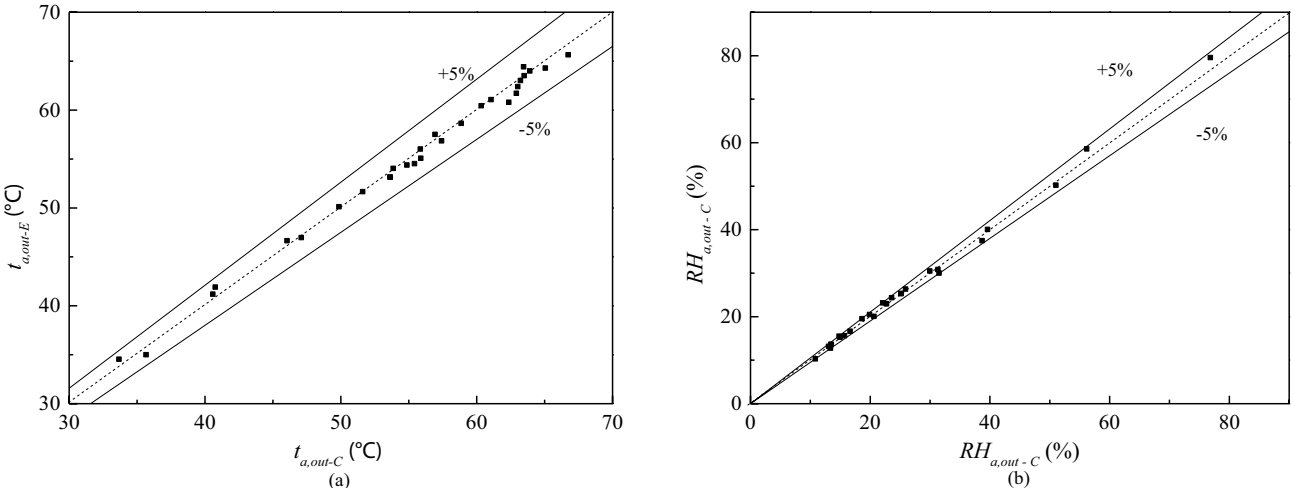

Fig. 8. Comparison between experimental results and simulated results of the spray separation tower: (a) outlet air temperature and (b) outlet air relative humidity.

wastewater inlet temperature, air mass flow rate, wastewater mass flow rate and mass concentration of the wastewater on the spray separation process are investigated by combining the simulation and experimental results.

4.2.1. Effects of air inlet temperature

Fig. 9a and b show the influence of air inlet temperature on the air outlet state of the tower and the evaporation rate of the spray separation tower and the moisture content of the outlet products respectively. With the increase of air inlet temperature, both air outlet temperature and moisture content of spray separation tower increase, but the rising trend is not linear. When the inlet air temperature exceeds 90°C, with the increase of air inlet temperature, the rise of air outlet temperature is significantly accelerated, while the rise of air outlet moisture content is somewhat slowed down.

This effect is reflected in the evaporation rate and the moisture content of the export product particles, that is, when the inlet air temperature exceeds 90°C, the evaporation rate of the spray separation tower gradually slows down with the increase of air temperature, while the moisture content of the export product particles decreases gradually. This is because, with the increase of air temperature, the moisture content of fog drops will gradually decrease. When the temperature exceeds 90°C, fog drops in the tower begin to crystallize gradually and form a solid phase on the surface. This phenomenon reduces the overall evaporation mass transfer coefficient of the tower, resulting in a slowdown in the increase of evaporation rate and water content decline rate.

In addition, the influence of air inlet temperature on the performance parameters of the spray separation tower is shown in Fig. 9c and d. The evaporation efficiency and energy efficiency of spray separation tower decrease with the increase of inlet air temperature. At the same time, when the air inlet temperature is less than 90°C, the evaporation energy efficiency and energy utilization rate do not decline significantly, while when the air temperature is more than 90°C (i.e., when solid products are gradually generated at the outlet of the spray separation tower), the EE_{ss} and EUR_{ss} decrease gradually and obviously. Although the increase of air inlet temperature can improve the evaporation rate of the spray separation tower, it will also lead to the decrease of the moisture content of the outlet particles (droplets). Therefore, the average mass concentration of droplets in the spray separation tower will also increase with the increase of air temperature, and the average partial surface water vapor pressure of fog drops will also decrease. The above comprehensive influence leads to the decline of evaporation energy efficiency and energy utilization ratio. In addition, when the air temperature exceeds 90°C, the

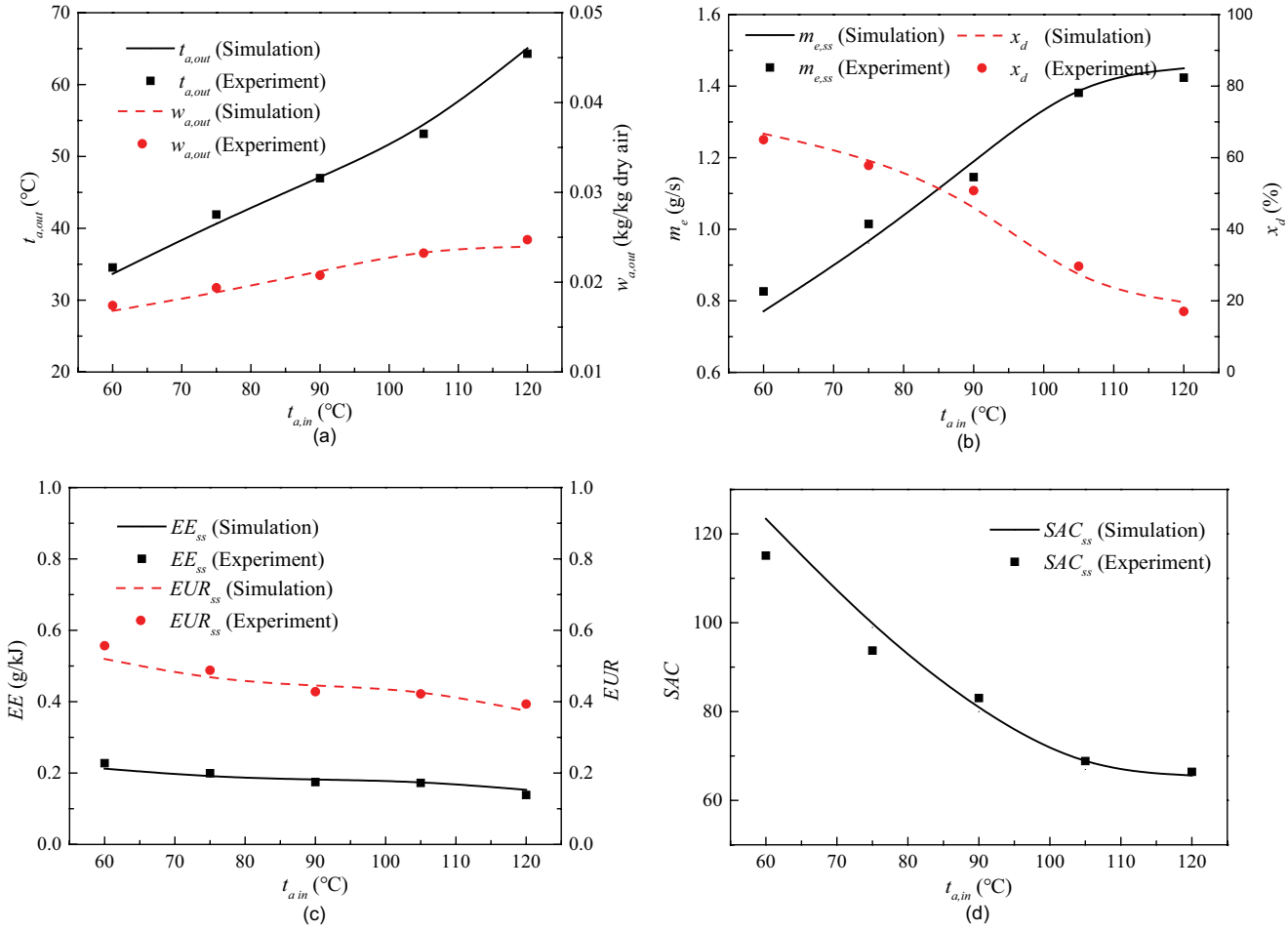

Fig. 9. Effects of air inlet temperature (a) air outlet temperature and air outlet humidity ratio; (b) evaporation rate and droplet moisture content; (c) EE and EUR; (d) SAC (m_d = 95.1 kg h^{-1}; m_w = 1.93 kg h^{-1}; $t_{w,in}$ = 22.7°C; x = 20%).

evaporation mass transfer process has further deteriorated with the gradual crystallization of the fog drops. Therefore, the further increase of air temperature will make the decline of evaporation energy efficiency and the energy utilization ratio of the spray separation tower more obvious. In addition, the increase in air temperature can reduce specific gas consumption. Therefore, the increase of air temperature can reduce the consumption of airflow, which is beneficial to the overall system in terms of reducing fan power.

4.2.2. Effects of inlet wastewater temperature

Fig. 10 shows the effect of the inlet temperature of wastewater on the spray separation tower. The change of wastewater temperature has little influence on air parameters, evaporation rate, evaporation efficiency and energy utilization. Although the increase of the inlet temperature of wastewater will increase the evaporation rate slightly, the promotion effect of the increase of the temperature of wastewater is not obvious because the flow rate of wastewater is relatively small compared with the flow rate of air. In addition, the improvement of wastewater temperature has little effect on evaporation efficiency and energy utilization but can reduce specific gas consumption. In general, the change of wastewater temperature has little influence on the whole spray separation process.

4.2.3. Effects of air mass flow rate

The influence of air mass flow rate is shown in Fig. 11. The increase of airflow rate will increase the air outlet temperature but decrease the moisture content at the air outlet. However, the reduction of moisture content at the air outlet did not inhibit the evaporation process, but promoted the evaporation rate and reduced the moisture content of the products at the outlet of the tower. This is due to the fact that, although the moisture content of the air outlet is reduced, the increased airflow also increases the heat carried into the spray separation tower, which promotes the overall evaporation of the spray separation tower.

For the heat and mass transfer performance of spray separation tower, the increase of airflow will lead to the decrease of evaporation energy efficiency and energy utilization ratio, and increase of specific gas consumption. Because, although the improvement of airflow promotes the improvement of evaporation rate, it also leads to the

increase of airflow rate inside the tower, reducing the retention time of fog drops inside the tower, and the air does not release its heat completely for mass transfer and evaporation. In addition, a higher airflow rate will reduce the moisture content of export products, and the crystallization solidification process in the tower will also reduce the mass transfer coefficient, thus reducing the average mass transfer driving potential in the spray separation process. The above variations also lead to the decrease of mass transfer efficiency of the evaporation process.

4.2.4. Effects of wastewater mass flow rate

The effect of wastewater mass flow rate is significantly different from that of airflow (Fig. 12). With the increase of wastewater flow, the air temperature at the outlet decreases and the moisture content increases. In addition, the increase of wastewater flow also promoted the increase of evaporation rate and the increase of moisture content of particles at the tower outlet. The increase of wastewater flow increases the number of droplets in the tower, as well as the heat and mass transfer surface area in the tower, which promotes the evaporation process. At the same time, the increase of wastewater flow also reduced the average concentration of droplets in the tower and increased the mass transfer driving potential in the evaporation process. The above phenomena can also be explained by Fig. 12c. The increase of wastewater flow leads to the improvement of evaporation efficiency and energy utilization rate. In addition, the increase in wastewater flow will also lead to an increase in specific gas consumption. It can be seen that the flow of wastewater and airflow are exactly the opposite.

4.2.5. Effects of the mass concentration of the wastewater

The influence of the mass concentration of the wastewater in the spray separation tower is shown in Fig. 13. The increase of mass concentration of the wastewater will lead to the increase of outlet air temperature and the decrease of outlet air moisture content. The increase of mass concentration of the wastewater can lead to the decrease of steam partial pressure on the surface of the droplet in the tower, thus reducing the mass transfer driving potential in the evaporation separation process. Therefore, the increase of mass concentration of the wastewater also leads to the decrease of evaporation rate, as shown in

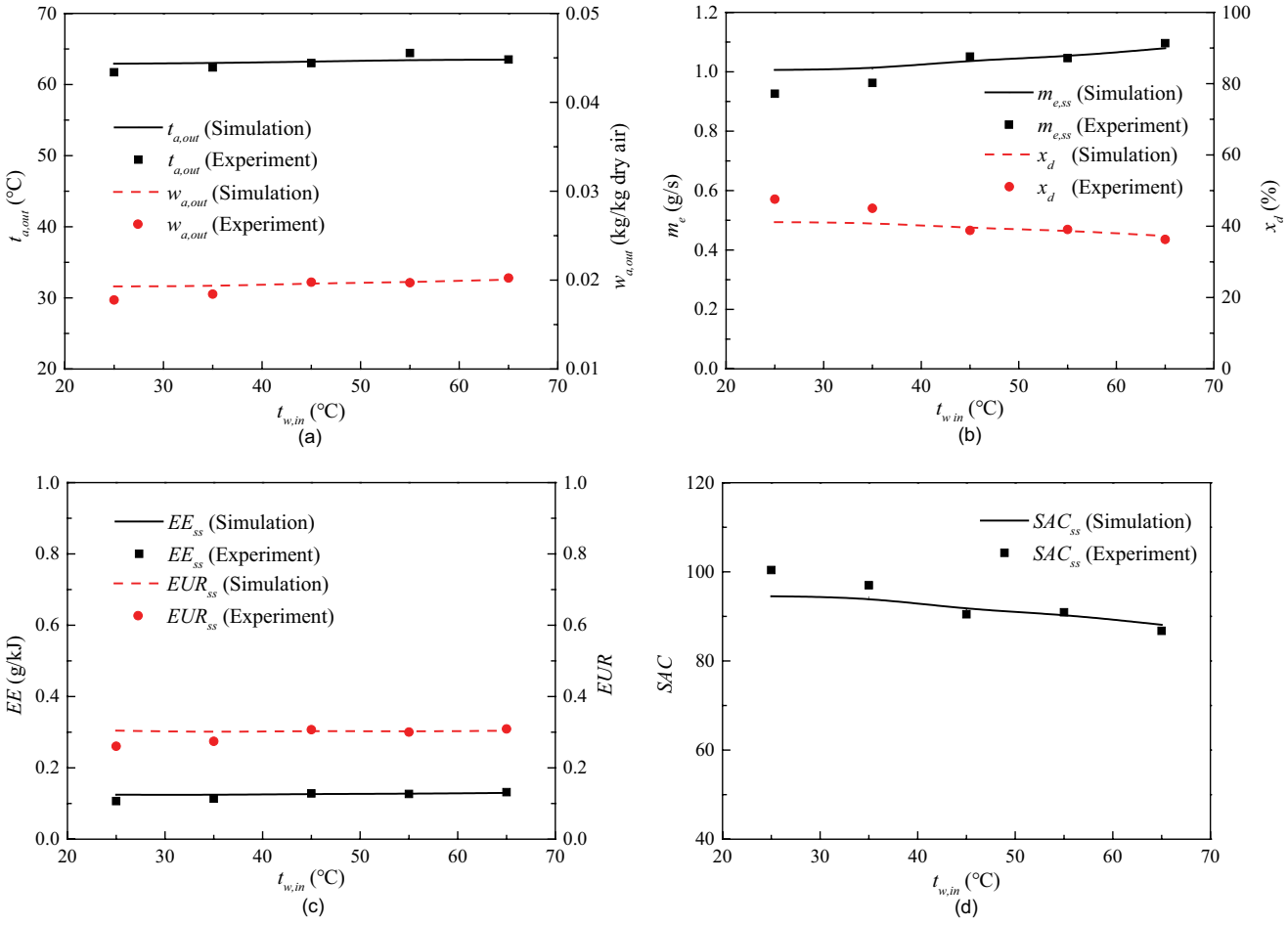

Fig. 10. Effects of wastewater inlet temperature (a) air outlet temperature and air outlet humidity ratio; (b) evaporation rate and droplet moisture content; (c) EE and EUR; (d) SAC (m_d = 95.1 kg h^{-1}; m_w = 2.187 kg h^{-1}; $t_{a,in}$ = 105°C; x = 31.77%).

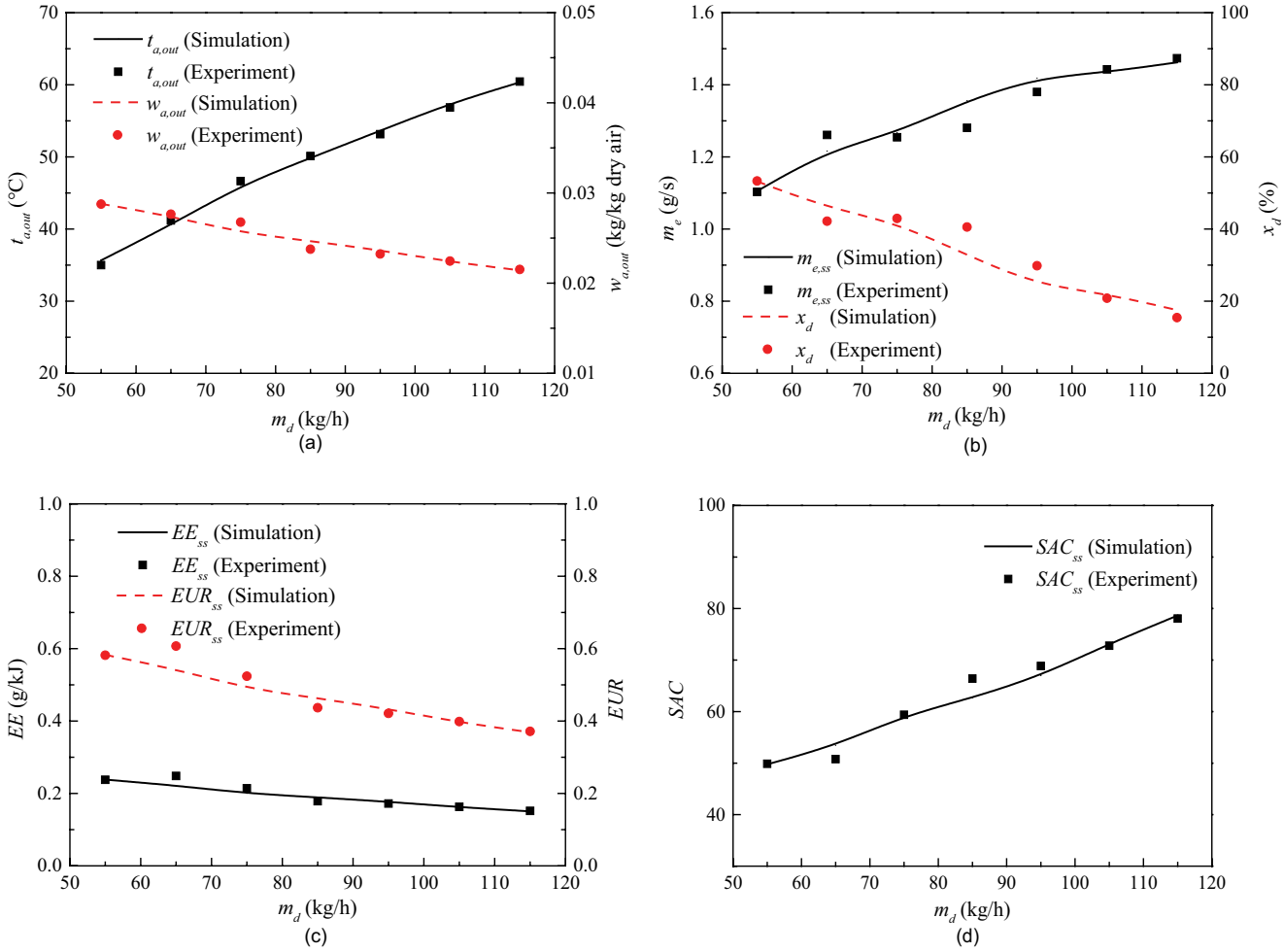

Fig. 11. Effects of air mass flow rate (a) air outlet temperature and air outlet humidity ratio; (b) evaporation rate and droplet moisture content; (c) EE and EUR; (d) SAC (m_w = 1.93 kg h^{-1}; $t_{a,in}$ = 105°C; $t_{w,in}$ = 22.6°C; x = 20%).

Fig. 13b. However, the increase of mass concentration of the wastewater is indeed conducive to the solidification and crystallization process. With the increase of mass concentration of the wastewater, the moisture content of the products at the outlet of the tower will gradually decrease. When the concentration at the inlet of the wastewater solution is greater than 30%, the spray separation tower under this working condition basically reaches the limit of drying crystallization, and the moisture content of the export product is basically not reduced.

As for the energy efficiency of spray separation tower, the improvement of mass concentration of the wastewater will lead to the reduction of evaporation energy efficiency and tower energy utilization rate, as well as the increase of specific gas consumption. It is obvious that the increase of mass concentration of the wastewater will inhibit the evaporative mass transfer process. Nevertheless, the improvement of mass concentration of the wastewater is the key to complete the dry crystallization process. Although the solution with low concentration can ensure efficient evaporation and mass transfer, it cannot realize the solidification of the droplet, and the energy efficiency caused by the increase of concentration is not obvious. Therefore, the concentration of the spray separation process should be selected to reduce the concentration of the solution as much as possible while ensuring the completion of curing and crystallization at the exit of the tower.

Based on the analysis of the above five main factors, it can be found that for the evaporation separation process in the spray separation tower whether solid crystallization products can be formed, the most important influencing factor is the air inlet temperature, followed by the concentration of wastewater. The influence of airflow and wastewater flow is more to match the necessary latent heat required for evaporation in the tower. The effect of wastewater temperature is minimal. Under specific flow conditions, whether the spray separation tower can realize the solidification process of crystallized salt depends on whether the air inlet temperature is high enough. At the same time, increasing the concentration of imported wastewater can effectively promote the solidification crystallization of the evaporation separation process. However, in terms of energy efficiency, premature solidification crystallization in the tower will

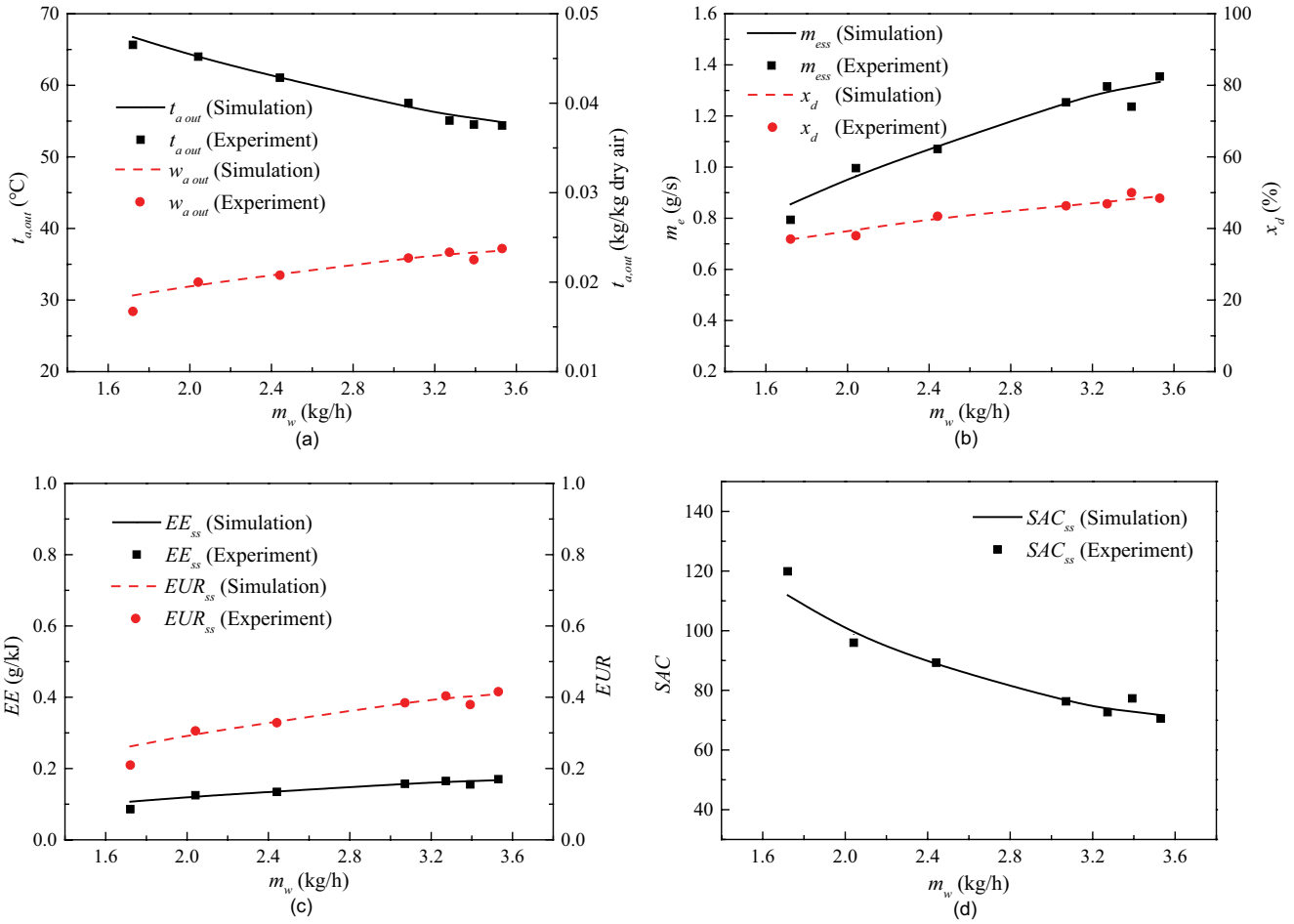

Fig. 12. Effects of wastewater mass flow rate (a) air outlet temperature and air outlet humidity ratio; (b) evaporation rate and droplet moisture content; (c) EE and EUR; (d) SAC (m_d = 95.6 kg h^{-1}; $t_{a,\text{in}}$ = 105°C; $t_{w,\text{in}}$ = 23.7°C; x = 31.77%).

inevitably lead to the decrease of the overall average mass transfer coefficient and mass transfer drive potential of the spray separation tower, as well as the decline of evaporation energy efficiency and energy utilization of the spray separation tower. Therefore, on the premise that evaporation crystallization can be realized at the bottom of the tower, the energy efficiency of the tower can be improved to a certain extent by appropriately reducing the concentration of wastewater inlet and the temperature of the air inlet. In addition, the increase in air temperature can reduce the specific gas consumption of the spray separation tower. For this system, the reduction of specific air consumption can make it possible to select a fan with a smaller power under the same working condition.

In summary, it can be concluded that maintaining an appropriate air inlet temperature can not only guarantee the solidification and crystallization of droplets at the exit of the spray separation tower but also maintain relatively high thermal efficiency and energy utilization rate of the spray separation tower.

Table 6 summarizes the corresponding relationship between the solidification and crystallization of droplets in the spray separation tower and the energy efficiency of the spray separation tower at different inlet air temperatures when the mass concentration of the wastewater is 20%. It can be seen that when the air inlet temperature is greater than 90°C, the wastewater droplets at the outlet of the spray separation tower can already reach the state of solidification and crystallization. However, with the gradual increase of the air inlet temperature, the thermal efficiency and energy utilization rate of the spray separation tower will gradually decrease. When the temperature is greater than 105°C, the decrease rate will also be significantly accelerated. Therefore, it is necessary to maintain the air temperature within a reasonable range (for example, when the wastewater mass concentration is 20% here, 105°C > $t_{a,\text{in}}$ > 90°C) under the premise of ensuring that the tower outlet can complete the curing crystallization of the wastewater droplets, which is beneficial to ensure the thermal efficiency and the energy utilization rate of the spray separation tower (for example, when the mass concentration is 20%, the thermal efficiency of the spray separation tower can be maintained above 70%, with a maximum of 71.97%, and the energy utilization rate of the spray separation tower can be maintained above 40%, with a maximum of 43.78%).

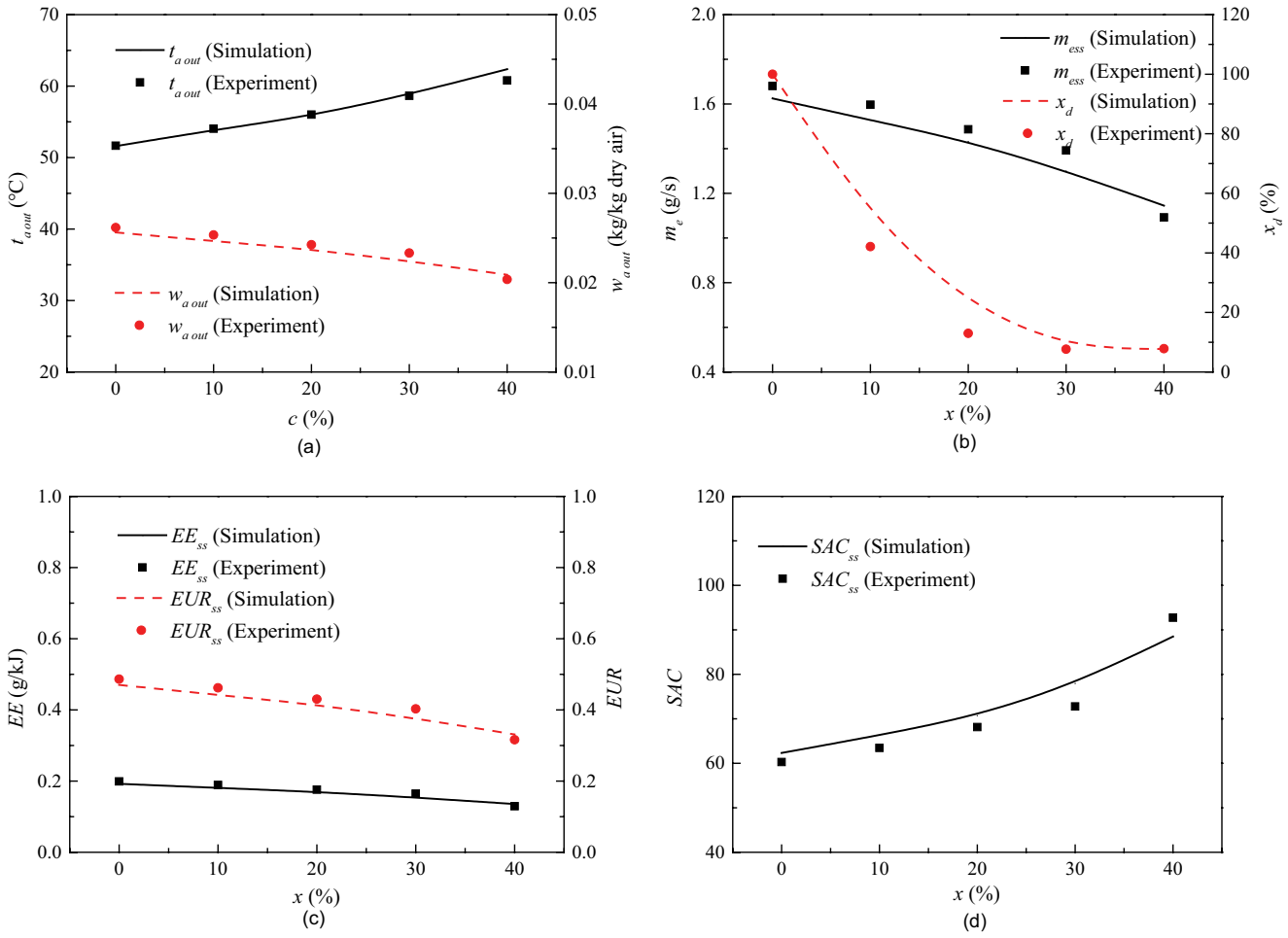

Fig. 13. Effects of the mass concentration of the wastewater (a) air outlet temperature and air outlet humidity ratio; (b) evaporation rate and droplet moisture content; (c) EE and EUR; (d) SAC (m_d = 101.3 kg h^{-1}; m_w = 1.93 kg h^{-1}; $t_{a,\text{in}}$ = 105°C; $t_{w,\text{in}}$ = 23.7°C).

Table 6
The corresponding relationship between the solidification and crystallization of droplets in the tower and the energy efficiency of the spray separation tower at different inlet air temperatures

Inlet air temperature (°C)	Whether there are crystals at the bottom of the tower	Thermal efficiency η_Q (kg/kg dry air)		Energy utilization rate (EUR, %)	
		Simulation results	Experimental results	Simulation results	Experimental results
60	No	75.07	77.25	51.97	54.69
75	No	71.99	73.67	46.21	47.78
90	Yes	71.07	71.97	44.41	43.78
105	Yes	70.88	70.33	43.36	42.17
120	Yes	67.67	68.14	37.42	39.33

4.3. Analysis of heat and mass transfer characteristics and droplet drying crystallization during the spray separation process

4.3.1. Variations of gas phase (air) in spray separation tower

As the carrier of spray separation evaporation and drying crystallization process, air plays the dual role of releasing heat (cooling) and absorbing water (moisture content increases). Figs. 14 and 15 show the changes in air temperature and air moisture content in the spray separation tower respectively. Compared with the lower air inlet temperature, the air in the spray separation tower can cool down more rapidly and release its own heat more quickly at high air inlet temperature. At the same time, the moisture content of the air increases more rapidly and the air absorbs

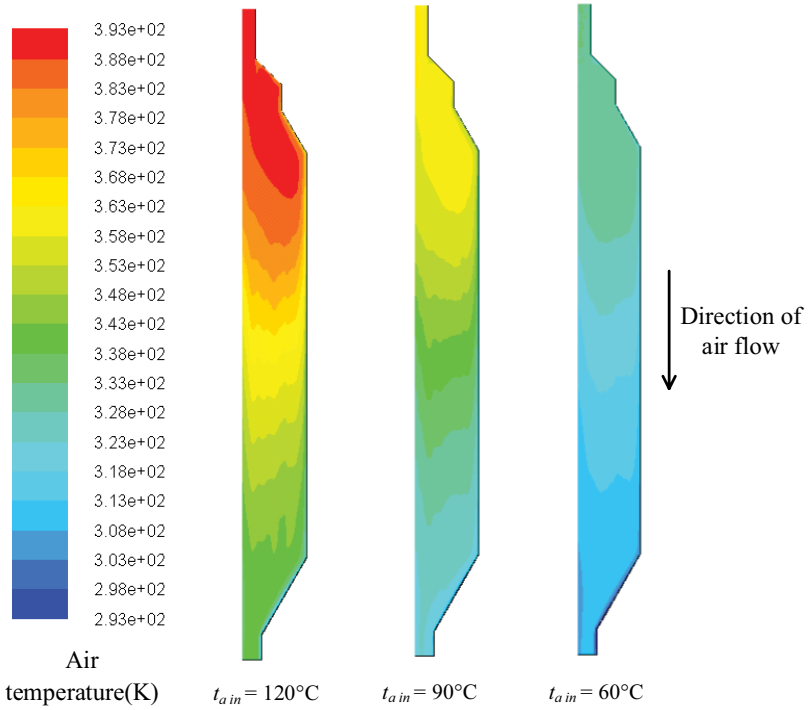

Fig. 14. Air temperature cloud diagram of spray separation tower.

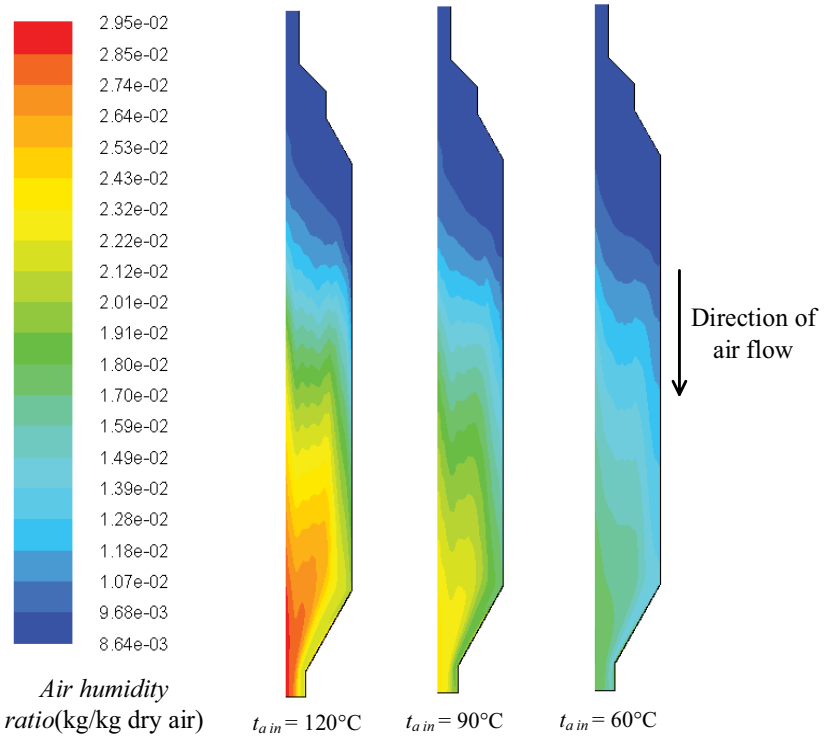

Fig. 15. Air humidity ratio cloud diagram of spray separation tower.

water more quickly. The decreasing range of air temperature gradually slows down with the flow direction, and the change of air moisture content also slows down with the flow direction. But the changes are slightly different.

The change of air temperature in the width direction of the tower is small, but the change of air moisture content in the width direction of the tower is large (especially in the middle and rear of the tower). This is because the gradual

structure at the bottom of the tower affects the spray flow pattern, which causes the droplets to adhere to the inclined plane. Meanwhile, the reduced structure also improves the air velocity near the axis. Both factors simultaneously lead to the high moisture content at the center and the low humidity content near the wall.

4.3.2. Variation of droplets in the spray separation tower

Fig. 16 shows the change of droplet's water content in the tower. Along with the direction of airflow, the moisture content of fog drops will continue to decline. However, when the inlet air temperature is high (120°C), the moisture content of droplets drops rapidly and the crystallization process is basically completed before reaching the inclined plane at the bottom of the tower. However, when the inlet temperature is 90°C, the moisture content of the fog drops at the inclined plane at the bottom of the tower is in a state between the beginning of precipitation of solid phase and complete drying crystallization. At this time, there is still a wet core inside the liquid drops and the fog drops are in an unstable hydrate state. However, when the inlet temperature of the tower drops to 60°C, the fog drops at the outlet of the tower are still in the liquid phase concentrated solution because the air temperature is not enough to realize the crystallization solidification process. In the direction of airflow, the moisture content of fog drops decreases slowly at the initial stage, then increases gradually, and then decreases gradually after the solid phase appears, finally tends to be stable. In the beginning, the water content of fog drops changed little, because, at this time, the water content of fog drops was higher, the water proportion was larger, and the relative decrease rate was slower. However, the evaporation rate was not low at this time.

In the direction of width, the water content of fog drops in the symmetrical center and near the wall of the tower is higher, while the water content in the middle area is lower. This is due to the higher air velocity at the symmetrical center of the tower (due to the tapered structure at the bottom of the tower), which leads to a shorter time for the droplet to stay at the center, so the droplet drying crystallization is slightly worse here. On the wall surface, because the sprayer will inevitably spray a small part of the fog drops on the wall surface, forming a falling film process, which will lead to the decrease of heat and mass transfer surface area, affecting the evaporation process of fog drops. Therefore, the water content of fog drops here will be higher than that of the central region.

Fig. 17 is the actual observation photo of the crystal products (fog drops) attached to the inclined plane at the bottom of the tower at 3 temperatures corresponding to Fig. 15. Consistent with the simulation results in Fig. 16, the dry crystal products obtained at three inlet air temperatures are respectively: dry crystal salt (calcium chloride dihydrate, white powder or agglomerated particle) corresponding to a thicker adhesion layer at 120°C; 90°C corresponds to the wet crystal salt in the thin layer (the product between calcium chloride dihydrate and calcium chloride hexahydrate; This part of the crystal after being removed from the tower to cool will absorb water from the air, forming hexahydrate calcium chloride transparent crystal salt); 60°C corresponds to the high concentration solution droplet that fails to complete the curing crystallization

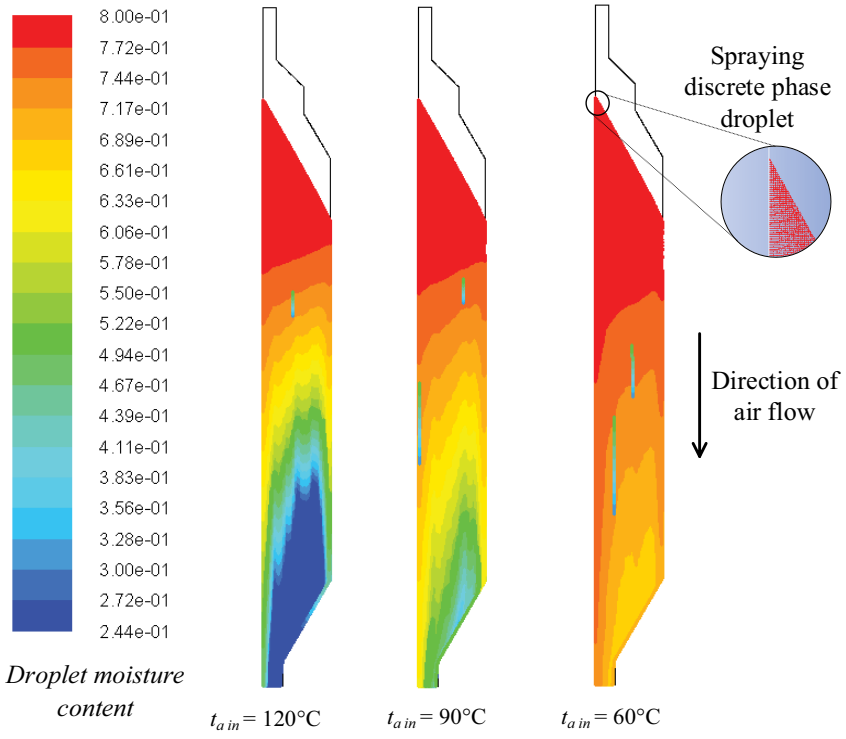

Fig. 16. Droplet moisture content cloud diagram of spray separation tower.

process. The actual picture of the recovered product after product sampling in the three cases is shown in Fig. 18.

4.3.3. Variation of in local instantaneous evaporation rate of droplets inside the spray separation tower

The local instantaneous evaporation rate of the droplets in the spray separation tower can be more intuitive to understand the specific intensity changes of the mass transfer process in the spray separation tower. Fig. 19 shows the changes of the local instantaneous evaporation rate along the airflow direction of the spray separation tower under three different inlet air temperatures. Under the three working conditions, the local instantaneous evaporation rate in the tower increases first and then decreases in the direction of airflow. The evaporation rate is 0 in the range of 2.575–2.225 m as the air is not in contact with the droplets. When the air reaches the height of 2.225 m of the tower, the air gradually comes into contact with the fog drops, the continuous phase air begins to transfer heat and mass with the discrete phase fog drops, and the evaporation rate gradually increases. However, the local evaporation rate increases slowly at this time because the droplets are not completely dispersed and cover the entire diameter range of the tower. As the droplets gradually dispersed, the local evaporation rate within the tower increased rapidly, reaching its maximum height when the tower was about 1.7 m. As the evaporation separation process goes on, the concentration of the droplets in the wastewater solution gradually increases, and the moisture content in the air gradually decreases, while the droplets are dispersed throughout the whole diameter of the tower. At this time, the local evaporation rate decreases stably under the influence of the partial pressure difference between the droplet and the air vapor, and the droplet evaporation process is in the stage of constant temperature evaporation. As the process continues (when the air inlet temperature is 120°C and 90°C), the local evaporation rate will drop sharply (when the temperature is 120°C: the tower height is within the range of 0.7~0.3 m; At 90°C, the height of the tower is 0.28~0 m. At this time, the decreased amplitude of the local evaporation rate was obviously larger than that at the constant temperature evaporation stage. At this time, the solid phase gradually began to precipitate out on the surface of fog drops, leading to a significant reduction in mass transfer coefficient, so the stage entered the stage of shell formation of fog drops and the drying stage of part of fog drops. When the evaporation separation process continue to develop, can enter the droplets are the final stage of drying (only appears at the inlet temperature of 120°C condition, the

$t_{a\,in}$ = 120°C $t_{a\,in}$ = 90°C $t_{a\,in}$ = 60

Fig. 17. Physical photographs of crystal (droplets) attachment on outlet slope of spray separation tower at different inlet air temperatures.

Dry crystalline salt (Calcium chloride dihydrate)

Cooled crystal salt (Calcium chloride hexahydrate)

Concentrated solution

Fig. 18. Physical photographs of three different products of spray separation tower.

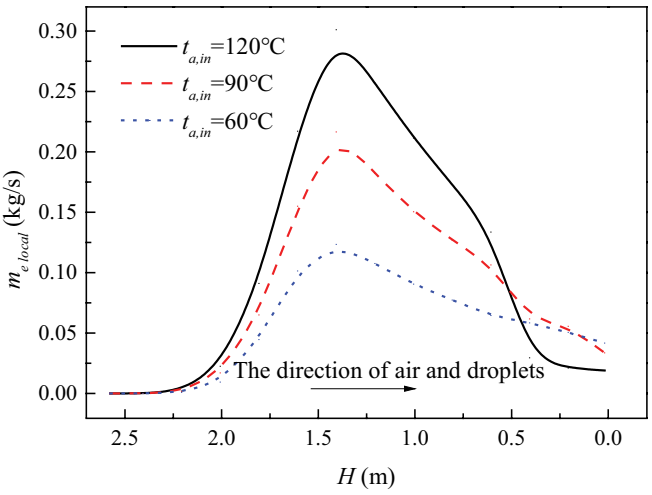

Fig. 19. The variation of local evaporation rate in the direction of airflow (opposite direction of tower height) in the spray separation tower.

height 0.3~0 m area), the tower evaporation rate in a very low level and will be slow to reduce, at this time due to droplets have completely into a shell, the process stage basic same as dry curing product drying process.

Based on the above analysis, it can be seen that although the solidified shell and drying process at the rear will inhibit the overall evaporation and mass transfer, so that the overall evaporation energy efficiency of the tower decreases. But increasing air inlet temperature is a necessary condition for droplet drying and curing. Therefore, in the design of the overall system, it is still necessary to select a larger air inlet temperature to ensure that the waste water products at the tower outlet can achieve the state of drying and curing.

5. Conclusion

In this paper, CFD simulation and experiment are combined to fully investigate the heat and mass transfer characteristics of air and wastewater droplets in spray separation tower and the evaporation drying and crystallization process of droplets. The CFD simulation model of spray separation tower is established based on the four-stage spray droplet drying model, and the performance experimental platform of spray separation tower is set up for experimental research. The accuracy of the spray separation tower model is verified by comparison test and simulation results (the maximum error of prediction of air temperature and air relative humidity are 4.83% and 5.19% respectively). Finally, according to the simulation and experimental results, the evaporation and heat and mass transfer characteristics of the spray evaporation separation process are analyzed, and the performance change law of this process is explored. The following conclusions are drawn:

- Air temperature has the greatest influence on the spray separation process. Increasing the air inlet temperature can increase the evaporation rate of the tower and reduce the moisture content of the tower outlet products. The temperature of spray solution has little effect on evaporation rate and moisture content of products
- The increase of air inlet temperature is not conducive to the evaporation efficiency and energy utilization rate of the tower, but can reduce the specific gas consumption of the spray separation tower.
- The concentration of wastewater also has a great influence on the spray separation process. The increase of concentration will lead to the decrease of evaporation rate, evaporation energy efficiency and energy utilization rate, resulting in the increase of specific gas consumption. Nevertheless, the increase of the mass concentration of the wastewater can reduce the evaporation load of spray separation tower and promote the decrease of moisture content of export products.
- It is necessary to maintain the air temperature within a reasonable range (when the x_{in} = 20%, 105°C > $t_{a,in}$ > 90°C) under the premise of ensuring that the tower outlet can complete the curing crystallization of the droplets, which is beneficial to ensure a high EUR (maintained above 40%, maximum of 43.78%) and η_Q (maintained above 70%, maximum of 71.97%).
- The heat and mass transfer processes in the spray separation tower are unified, both of which show that the heat and mass transfer process in the temperature adjustment and constant temperature evaporation stage is relatively intense, while the shell-forming stage gradually attenuates, and the drying stage is the lowest.
- Under different inlet temperatures, the product recovery and formation conditions are different. According to the form of product, it can be divided into three kinds: dry crystal salt, wet crystal salt and viscous salt solution. Among them, the dry crystal salt can be taken out and recycled directly, while the other two require secondary treatment (such as cooling crystallization) through subsequent subsidies.
- Improving air temperature can effectively improve the local evaporation rate of droplets in the tower before the shell-forming stage and promote mass transfer evaporation. At the same time, the tower export products to complete the drying curing process.

Acknowledgments

The authors gratefully acknowledge the financial support provided by Jiangsu Vocational Institute of Commerce for the present research work (Jiangsu Vocational Institute of Commerce, Startup Fund for PhD Talents; Number: 1042141223029).

Symbols

a_1, a_2 and a_3	—	Constant parameters for calculation of drag coefficient, –
A_p	—	Surface area of the droplet, m^2
C_D	—	Drag coefficient, –
C_p	—	Heat capacity, J mol^{-1} K^{-1}
C_s	—	Moisture concentration at the droplet surface, mol m^{-3}
C_∞	—	Moisture concentration in the bulk gas, mol m^{-3}
d_d	—	Droplet diameter, m
EE	—	Evaporation efficiency, kg kJ^{-1}

EUR — Energy utilization ratio, %
F — User-defined-function of additional forces, –
g — Acceleration of gravity, m s^{-2}
h — Convective heat transfer coefficient, W m^{-2} K^{-1}
h_{fg} — Specific latent heat, J kg^{-1}
i — Specific enthalpy, kJ kg^{-1}
i_0 — Specific enthalpy under the environment condition, kJ kg^{-1}
k — Turbulent kinetic energy, m^2 s^{-2}
k_c — Mass transfer coefficient, m s^{-2}
m_{cw} — Condensate water mass flow rate, kg s^{-1}
m_d — Air mass flow rate, kg s^{-1}
m_{dp} — Mass of droplet, kg
m_e — Evaporation rate, kg s^{-1}
m_{el} — Local evaporation rate, kg s^{-1}
m_w — Solution mass flow rate, kg s^{-1}
m_{w0} — Supplement solution mass flow rate, kg s^{-1}
P — Pressure, Pa
r — Radius of the tower, m
RH — Relative humidity, %
SAC — Specific air consumption, –
S_m — User-defined mass source, –
t — Centigrade temperature, °C
t_0 — Centigrade environment temperature, K
T — Absolute temperature, K
T_∞ — Gas phase temperature, K
T_0 — Environment temperature, K
v — Velocity, m s^{-1}
w — Humidity ratio, kg/kg dry air
x — Salt mass concentration of wastewater, %
z — Solid liquid area ratio on droplet surface, –

Greek

ε — Energy dissipation, m^2 s^{-2}
ρ — Density, kg m^{-3}
τ — Time, s
λ_∞ — Thermal conductivity of the gas phase, W m^{-1} K^{-1}
μ — Viscosity, kg m^{-1} s^{-1}
μ_t — Turbulent viscosity, kg m^{-1} s^{-1}

Subscripts

a — Air
cr — Wet nuclear
d — Droplet
in — Inlet of the tower
out — Outlet of the tower
r — Radial direction
ss — Spray separation process
w — Wastewater
x — Axial direction

Non-dimensional number

Nu — Nusselt number
Pr — Prandtl number
Re — Reynolds number
Sc — Schmidt number
Sh — Sherwood number

Acronyms

CFD — Computational fluid dynamics
DPM — Discrete phase model
HDH — Humidification–dehumidification
MEE — Multi-effect evaporation
MVR — Mechanical vapor recompression

References

[1] Y.T. Cai, The harm of electroplating wastewater on human body and its central treatment, Agro-Environ. Sci., 29 (2010) 205–208.
[2] L.Y. Chai, Q.Z. Li, Q.Q. Wang, X. Yan, Solid-liquid separation: an emerging issue in heavy metal wastewater treatment, Environ. Sci. Pollut. Res., 25 (2018) 17250–17267.
[3] W. Wang, H.J. Han, M. Yuan, H.Q. Li, F. Fang, K. Wang, Treatment of coal gasification wastewater by a two-continuous UASB system with step-feed for COD and phenols removal, Bioresour. Technol., 102 (2011) 5454–5460.
[4] H.J. Lu, J.K. Wang, J. Yu, Y.F. Wu, T. Wang, Y. Bao, D. Ma, H.X. Hao, Chemical engineering thermodynamics: Phase equilibria for the pseudo-ternary system ($NaCl+Na_2SO_4+H_2O$) of coal gasification wastewater at T = (268.15 to 373.15) K, Chin. J. Chem. Eng., 653 (2016) 955–962.
[5] A. Christ, K. Regenauer-Lieb, H.T. Chua, Boosted multi-effect distillation for sensible low-grade heat sources: a comparison with feed pre-heating multi-effect distillation, Desalination, 15 (2015) 32–46.
[6] M.A. Jamil, S.M. Zubair, Effect of feed flow arrangement and number of evaporators on the performance of multi-effect mechanical vapor compression desalination systems, Desalination, 429 (2018) 76–87.
[7] R.K. McGovern, G.P. Thiel, G. Prakash Narayan, S.M. Zubair, J.H. Lienhard V, Performance limits of zero and single extraction humidification–dehumidification desalination systems, Appl. Energy, 102 (2013) 1081–1090.
[8] L. Chen, C. Chen, J. Yu, S. Jin, Study on the heat and mass transfer characteristics of spray separation tower at low temperature and normal pressure, Int. J. Heat Mass Transfer, 153 (2020) 119662, doi: 10.1016/j.ijheatmasstransfer.2020.119662.
[9] S. Wang, T. Langrish, A review of process simulations and the use of additives in spray drying, Food Res. Int., 42 (2009) 13–25.
[10] F.Y. Zhang, H. Hao, X. Li, H.-X. Li, Y.L. Zhao, Study on spray-drying process for waste liquor from paper mill, Chem. Eng. (China), 36 (2008) 1–4.
[11] T. Rouissi, A. Mahmoudi, R.D. Tyagi, S.K. Brar, D. Prèvost, R.Y. Surampalli, Optimisation of spray drying by response surface methodology for the production of *Sinorhizobium meliloti* powder formulation by using starch industry wastewater, Biosyst. Eng., 114 (2013) 334–343.
[12] A.N. Chasekioglou, A.M. Goula, K.G. Adamopoulos, H.N. Lazarides, An approach to turn olive mill wastewater into a valuable food by-product based on spray drying in dehumidified air using drying aids, Powder Technol., 311 (2017) 376–389.
[13] L. Chen, Investigation on Performance of Heat Pump Air Circulation Evaporation Separation System for Plating Wastewater, Nanjing Tech University, Nanjing, 2020.
[14] S.A. El-Agouz, G.B. Abd El-Aziz, A.M. Awad, Solar desalination system using spray evaporation, Energy, 76 (2014) 276–283.
[15] A. Fouda, S.A. Nada, H.F. Elattar, S. Rubaiee, A. Al-Zahrani, Performance analysis of proposed solar HDH water desalination systems for hot and humid climate cities, Appl. Therm. Eng., 144 (2018) 81–95.
[16] F. Farahbod, D. Mowla, M.R. Jafari Nasr, M. Soltanieh, Experimental study of forced circulation evaporator in zero discharge desalination process, Desalination, 285 (2012) 352–358.
[17] X.N. Fei, C. Lei, D. Yuman, J. Min, J.P. Fu, CFD modeling and analysis of brine spray evaporation system integrated with solar collector, Desalination, 366 (2015) 139–145.

[18] Q. Chen, M. Kum Ja, Y. Li, K.J. Chua, Evaluation of a solar-powered spray-assisted low-temperature desalination technology, Appl. Energy, 211 (2018) 997–1008.
[19] J. Yu, S.M. Jin, Y.J. Xia, Experimental and CFD investigation of the counter-flow spray concentration tower in solar energy air evaporating separation saline wastewater treatment system, Int. J. Heat Mass Transfer, 144 (2019) 118621, doi: 10.1016/j.ijheatmasstransfer.2019.118621.
[20] R.J. Moffat, Describing the uncertainties in experimental results, Exp. Therm. Fluid Sci., 1 (1988) 3–17.
[21] M.H. Sadafi, I. Jahn, A.B. Stilgoe, K. Hooman, Theoretical and experimental studies on a solid containing water droplet, Int. J. Heat Mass Transfer, 78 (2014) 25–33.
[22] S.A. Morsi, A.J. Alexander, An investigation of particle trajectories in two-phase flow systems, J. Fluid Mech., 55 (1972) 193–208.
[23] S.S. Sazhin, Advanced models of fuel droplet heating and evaporation, Prog. Energy Combust. Sci., 32 (2006) 162–214.
[24] A.S. Mujumdar, Handbook of Industrial Drying, 4th ed., CRC Press, Boca Raton, BR, USA, 2014.
[25] T.T.H. Tran, M. Jaskulski, J.G. Avila-Acevedo, E. Tsotsas, Model parameters for single-droplet drying of skim milk and its constituents at moderate and elevated temperatures, Drying Technol., 35 (2017) 444–464.
[26] M.H. Sadafi, I. Jahn, A.B. Stilgoe, K. Hooman, Theoretical and experimental studies on a solid containing water droplet, Int. J. Heat Mass Transfer, 78 (2014) 25–33.